BIOCOMPATIBLE AND BIOMIMETIC SELF-ASSEMBLY OF FUNCTIONAL NANOSTRUCTURES

The Air Force Office of Scientific Research Project Number FA9550-07-1-0054

PI: C. Jeffrey Brinker, Distinguished and Regent's Professor, Department of Chemical and Nuclear Engineering, The Department of Chemistry, and The Department of Molecular Genetics and Microbiology, the University of New Mexico, Albuquerque, NM 87131 Fellow, Sandia National Laboratories, Albuquerque, NM 87185

Program Manager: Dr. Hugh DeLong, Surface and Interfacial Science,

AFOSR, Arlington, VA 22203-1954

REPORT DOCUMENTATION PAGE

Form Approved
OMB No. 0704-0188

1. REPORT DATE *(DD-MM-YYYY)*	2. REPORT TYPE	3. DATES COVERED *(From - To)*
28-02-2010	Final	Dec 2006 - Nov 2009

4. TITLE AND SUBTITLE
BIOCOMPATIBLE AND BIOMIMETIC SELF-ASSEMBLY OF FUNCTIONAL NANOSTRUCTURES

5a. CONTRACT NUMBER
FA9550-07-1-0054

5b. GRANT NUMBER
FA9550-07-1-0054

5c. PROGRAM ELEMENT NUMBER

6. AUTHOR(S)
Carnes, Eric. C.; Brinker, C. Jeffrey

5d. PROJECT NUMBER

5e. TASK NUMBER

5f. WORK UNIT NUMBER

7. PERFORMING ORGANIZATION NAME(S) AND ADDRESS(ES)
Regents of the University of New Mexico
Special Assistants to the VP for Research and Economic Development, MSC01 1247
1 University of New Mexico
Albuquerque, NM 87131-0001

8. PERFORMING ORGANIZATION REPORT NUMBER
06410 AFOSR

9. SPONSORING/MONITORING AGENCY NAME(S) AND ADDRESS(ES)
Air Force Office of Scientific Research
Arlington, VA 22203-1954

10. SPONSOR/MONITOR'S ACRONYM(S)
AFOSR

11. SPONSORING/MONITORING AGENCY REPORT NUMBER

12. DISTRIBUTION AVAILABILITY STATEMENT
Approved for public release; distribution is unlimited.

13. SUPPLEMENTARY NOTES

14. ABSTRACT

We have discovered and continue to explore a unique metabolically and optically controlled lithography approach that allows patterned integration of live cells into nominally solid-state devices and maintains their viability under extreme conditions of desiccation and starvation. We used our cellular integration approach to explore quorum sensing at the individual cell level. We have also developed techniques for the integration of mammalian cells into devices. We continue to create biocompatible cellular microenvironments with tailored chemical and physical properties that direct cellular behavior. In summary our research provides a means to integrate cells into devices and platforms, maintain their viability under harsh conditions, and direct their behavior thorough engineered microenvironments.

15. SUBJECT TERMS
nanotechnology, biotechnology, bio/nano interface, cell immobilization, sol-gel, self-assembly, biosensor, quorum sensing

16. SECURITY CLASSIFICATION OF:			17. LIMITATION OF ABSTRACT	18. NUMBER OF PAGES	19a. NAME OF RESPONSIBLE PERSON
a. REPORT	b. ABSTRACT	c. THIS PAGE	UU	45	C. Jeffrey Brinker
U	U	U			19b. TELEPONE NUMBER (*Include area code*) 505-272-7627

1. Overview

Biological systems have evolved to perform complex functions like molecular detection, replication, and repair. To develop life-like qualities in synthetic materials, recent research has focused on incorporation of biomolecules, while incorporation of living organisms is less well studied. Furthermore in areas like cell-based sensing little effort has been made to replicate the nanoscale structure of the extra-cellular matrix (ECM). This is problematic in that cells are inherently sensitive to local nano-to-micro-scale patterns of chemistry and topography. Our proposed research exploits our recent discovery of the ability of living cells to organize extended nanostructures and nano-objects in a manner that creates a unique, highly biocompatible bio/nano interface, mimicking the ECM. Using amphiphilic phospholipids to direct inorganic self-assembly in the presence of living cells, we found that yeast and bacterial cells intervene, re-directing the assembly process to form a fluid, multi-layered lipid interface at the cell surface that interfaces coherently with an ordered lipid/silica nanostructure. Remarkably this hybrid structure maintains fluidic accessibility and cell viability even after evacuation and electron imaging. Using printing and patterning techniques developed previously by us for inorganic nanostructures, we can integrate cells into platforms needed for electronic, optical, and spectroscopic interrogation. Using this 'cell-directed assembly' approach, we have advanced the discovery and integration of new classes of nominally solid-state materials and devices displaying a symbiotic relationship between the biotic and abiotic components. Materials classes include, but are not limited to: cellular arrays fabricated with precise control of cell density and spacing allowing the development and interrogation of cell-to-cell communication networks associated with quorum sensing, biofilm formation, and many physiological events in pathogenic bacterial infections, and biosensensors for biological/chemical warfare agent detection in extreme environments utilizing extremophile organisms and components. This research has allowed us to extend the cell-directed assembly process to create new, functional bio/nano interfaces and biotic/abiotic materials. By introducing natural, non-native, and even inorganic materials into these interfaces, we can create hybrid materials capable of tailorable complex functions. These materials, representing the integration of biological functionality into nano- and micro- scale systems, have a wide range of uses, including: cell-based sensing in extreme environments; new, sensitive cellular interrogation and imaging systems; general platforms for understanding and exploiting cell-cell communication including disease, injury, and therapy; and the creation of "living materials" which sense and respond to their environment through the integration of living organisms.

.

2. Accomplishments and New Discoveries

2.1 Inclusion of multiple amphipathic components to control and tailor interfacial structure and function

Cellular plasma membranes incorporate multiple amphipathic components, including phospho- and glycolipids, cholesterol, and integral and peripheral proteins. Our previous work has focused on using single, short chained lipid species as (nano)structure directing agents, where the size and shape of the lipids establish the dimensional scale and morphology of the surrounding silica nanostructure. We expect that CDA conducted with lipid mixtures (and optionally cholesterol and proteins) will enhance cell viability and allow selective lipid partitioning at the cellular interface, raft formation, and the localization of non-native transmembrane proteins. This in turn should influence membrane fluidity, chemical gradient development, transport of molecules and signals, and membrane healing. Additionally we expect to be able to use the nanostructured host as a reservoir for nutrients and growth factors to control metabolic activity. Finally through control of the pore size, surface chemistry, and connectivity of the nanostructured host we expect to engineer transport characteristics important to cell-cell signaling.

In order to understand CDA and explore its ability to develop more complex and functional interfaces and matrices (mimicking on some level the ECM), we have employed a series of water soluble *di*C_6 lipids as structure directing agents and have monitored the evolving structure with fluorescence microscopy and GISAXS. Figure 1, shows confocal images of yeast immobilized within silica matrices where we included 1% of the corresponding optically labeled lipid analog. We observe that different lipid headgroups result in quite different bio/nano interfaces. Most dramatically switching from phosphotidyl choline (PC) to phosphotidyl ethanolamine (PE) results in an interface where there is no apparent preferential lipid localization. In that the pK_a of these headgroups is similar within half a unit, these results indicate that the cell/lipid interaction (and resulting interface) cannot be explained strictly by electrostatics. GISAXS studies of this system showed that the PE headgroup also did not 'switch' the nanostructure from 2D hexagonal to lamellar as observed for PC (see CJB *et al*. *Science* 2006). To fundamentally understand the lipid headgroup/cellular interaction, we are initiating laser tweezer and AFM studies of the effective interaction potential between cells and model supported lipid bilayer systems, lipid bilayer coated beads or supported lipid bilayers, respectively.

To introduce other non-soluble, biologically relevant lipids for CDA, we have prepared water-soluble liposomes that were then introduced during the standard CDA process (with or without additional transmembrane proteins). Figure 2 shows confocal slices of a system prepared with 1% NBD-labeled *di*C_6PC plus POPC liposomes optically labeled with 1% of Texas red labeled DHPE. We observe that both the short chain *di*C_6PC structure directing lipid and the longer chained POPC lipids are localized at the cellular surface. The merged image however suggests that the longer chain lipid is preferentially localized at the cellular interface as well as the interface with the surrounding silica nanostructure (black in image).

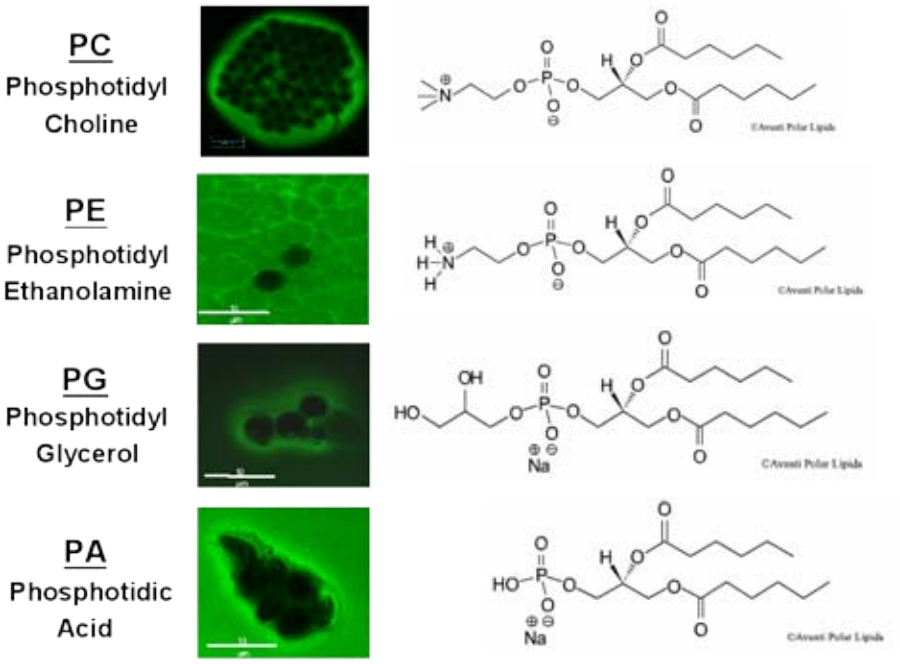

Figure 1. Flourescence confocal images of optically labeled C_6 lipids used in cell directed assembly. Different lipid headgroups result in vastly different extents of lipid localization at the cellular interface (yeast cells appear black).

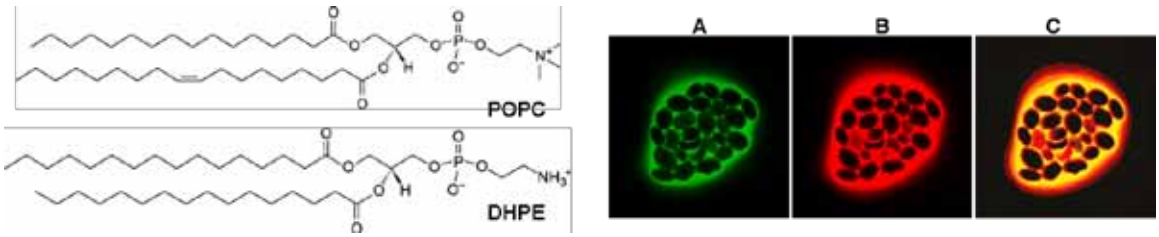

Figure 2. Confocal fluorescence slices of yeast immobilized in *di*C6PC (labeled green) templated silica matrices prepared using CDA with added POPC liposomes. Liposomes included 1% Texas red labeled DHPE, which presumably tracks the location of POPC. Red rims located at the cellular surfaces and at the interface with the surrounding silica matrix (black) suggest preferential lipid localization.

2.2 Creating new interfaces by incorporating non-native functional proteins to yield new functionality

Attempts to physically modify the cell surface and introduce new functionality through the integration of non-native proteins have seldom been successful due to the complexity associated with proteins and cells. Therefore, cell modification is usually accomplished via labor intensive, time consuming and expensive genetic modifications. Genetic engineering techniques require extensive specialization, and although considerable progress has been made in genomics and proteomics, there are still numerous physical barriers to overcome when attempting to introduce foreign functionality across cell species and kingdoms. During the past year, we have demonstrated a novel technique that utilizes our CDA process to physically

introduce functional bacterial proteins at the surface of yeast cells. Bacteriorhodopsin (BR) is a transmembrane photochromic protein isolated from the purple membrane of the salt marsh halophile, *Halobacterium salinarum.* It acts as an energy transducer, absorbing and converting light into chemical energy. We have introduced BR in to our CDA systems using two approaches: addition of the purified protein directly or incorporation of the BR into a DMPC liposome. Figure 3A-C show that adding the protein directly results in BR localization in a somewhat diffuse region that corresponds closely to the region of *di*C_6PC lipid localization. Figure 3D-F show that introduction of BR in a liposome results in a more conformal region of BR localization and that the longer chain DMPC (labeled green in these panels) preferentially localizes at the cellular surface (consistent with Figure 2). Because BR (and more generally transmembrane protein) functionality requires incorporation in a lipid bilayer with the structure/dimension needed to accommodate the hydrophilic and phobic domains, we hypothesized that, to function as a protein pump, BR would have to be incorporated in a longer chain lipid bilayer. Figure 4 shows pH gradient development for these two approaches. We find that BR introduced in a liposome dramatically changes the pH gradient. This suggests the BR is functional and preferentially oriented at the cellular surface. These results point out a completely new approach in which proteins with unusual properties can be isolated from one organism and physically introduced at the surface of another organism to provide new non-native functionalities.

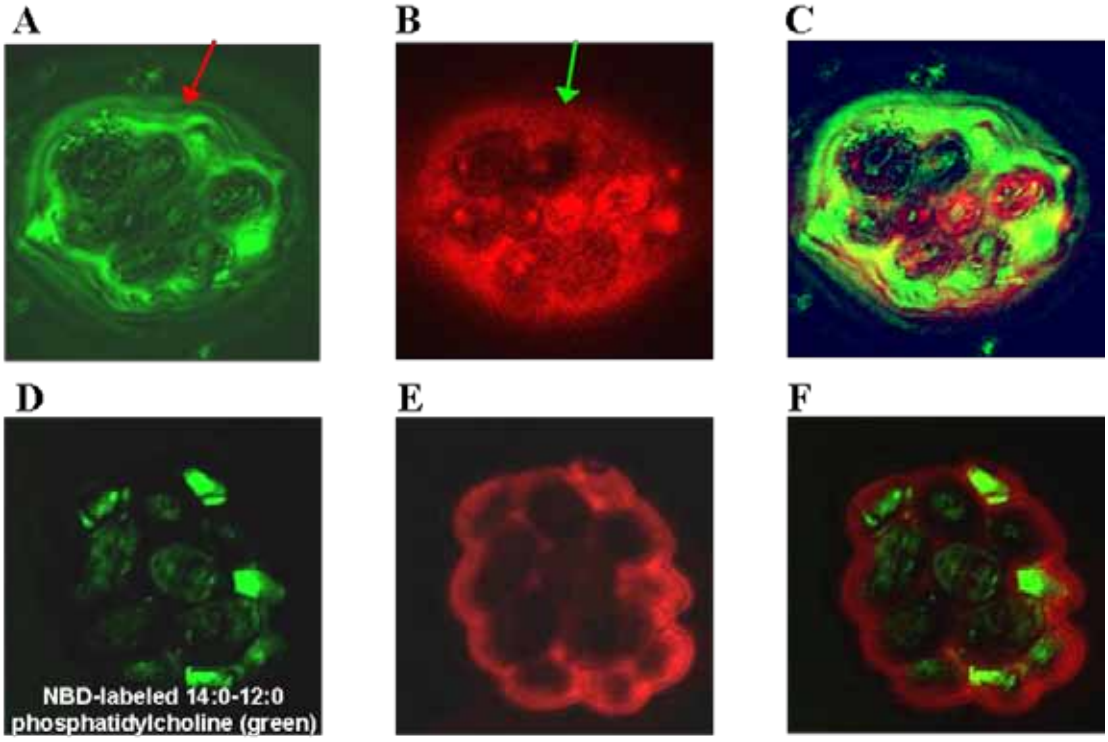

Figure 3. Confocal fluorescence slices of red emission fluorophore labeled Bacteriorhodopsin (BR) localized around yeast cells using cell-directed assembly. (A-C) BR added directly during CDA where the green label is on the *di*C_6PC structure directing agent. (D-F) BR added from liposome. (D) fluorescently labeled POPC lipid (green). (E) Fluorescently labeled Bacteriorhodopsin (red) and (F) a merged image showing co-localization of the lipid and

protein around the cells. These three panels show that POPC is preferentially localized at the cell surface. BR incorporation in POPC should allow it to achieve its native functionality.

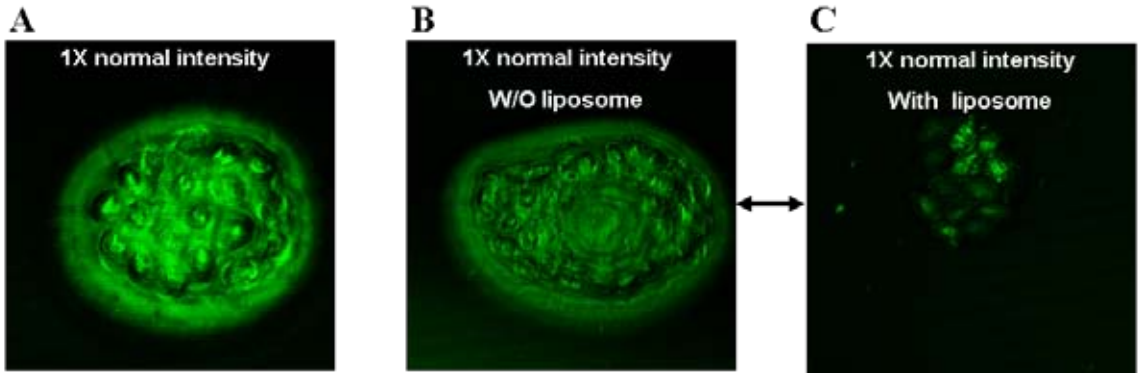

Figure 4. Comparison of pH gradient development with: (A) yeast prepared by CDA, (B) BR added directly during CDA, (C) BR introduced in liposome. The labeled dye is pH sensitive and lower pH results in weaker fluorescence.

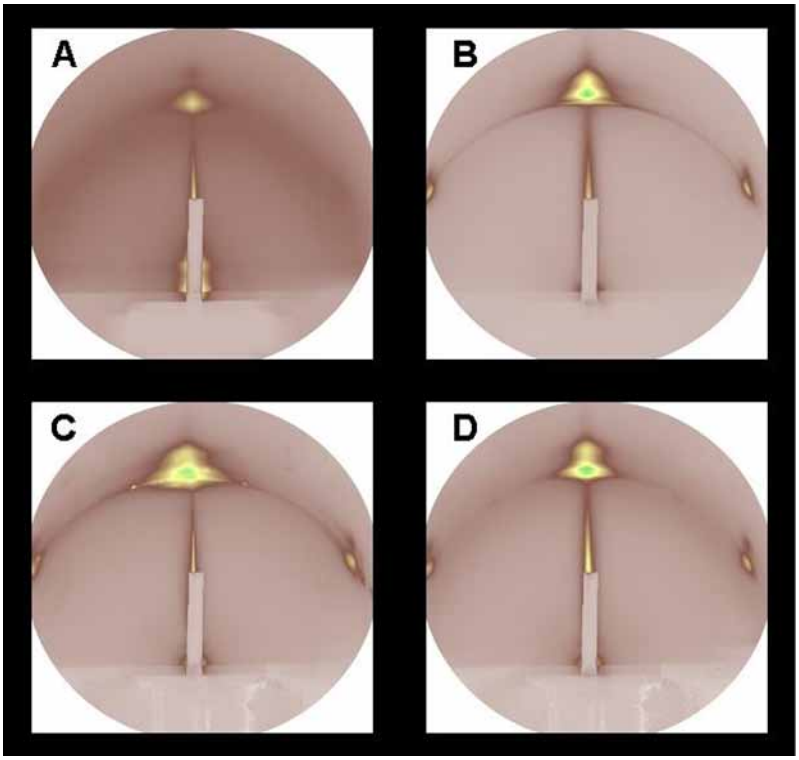

Figure 5. GISAXS patterns of various cell types immobilized using CDA: (A) *S. cerevisiae*, (B) *E. coli*, (C) *B. subtilis*, (D) *T. aquaticus.* Patterns B-D represent a 2D hexagonal mesophase. Pattern A is that of a lamellar

mesophase. Finer scale details of the 2D spot patterns are presumably associated with the detailed structure of the bio/nano interface.

2.3 Extension to various microorganisms

To extend the applicability of our CDA process, we have continued to explore the structure and properties of systems prepared with new organisms and cells - model organisms which provide a baseline to understand the influence of nanostructuring on cellular behavior, unique organisms which may allow the development of unprecedented functions in cell-based devices, and mammalian cells. For example, we have demonstrated CDA with a model eukaryote, *S. cerevisiae*, a model gram-negative bacterium, *E. coli*, and a model gram-positive bacterium *S. epidermidis*. We have also investigated CDA with the anthrax analogue *B. subtilis* for potential biodefense studies, the tuberculosis analogue *M. smegmatis* for potential infectious disease studies, as well as extremophiles like *T. auquaticus*, which lives in high-temperature environments, and *D. radiodurans*, which withstands extraordinary exposures to DNA damaging radiation. We find that all these microorganisms can be successfully immobilized via CDA. However each organism or cell displays its own unique behavior/interface. We have studied these interactions using grazing-incidence small-angle X-ray scattering at the Advanced Photon Source at Argonne National Laboratories (Figure 5). We find that each cell type has a unique ability to localize the lipid surfactant and establish local pH and ion gradients that in turn effect the development of the silica nanostructure probed by GISAXS. In particular extensive lipid localization at the yeast surface is correlated with the switching of the 2D hexagonal mesophase to a lamellar mesophase, which is not observed for organisms which exhibit lower extents of lipid localization.

2.4 Extension to model mammalian cells

Our previous research has demonstrated CDA as a general immobilization route for various single-celled organisms. To enhance the viability of immobilized cells, we have investigated new media in which to conduct CDA that incorporate essential nutrients and allow the nanostructured silica host to serve as a nutrient reservoir. In this fashion we maintain cellular access to necessary resources and avoid the requirement for constant regeneration of nutrients common to all other cell immobilization techniques to date. Supply of nutrients is especially important for extending CDA to mammalian cell lines. Whereas single-celled organisms can senesce, or pause their metabolic activity until more nutrients are available, mammalian cells quickly expire without constant access to nutrients and other chemical factors. We expect immobilization of mammalian cells to be important for tissue engineering, directing cell differentiation, and studying the onset of disease.

We have used CDA to incorporate model mammalian cells, such as adherent human embryonic kidney (HEK) cells, into our lipid-templated host nanostructures and have found that mammalian cells localize and internalize fluorescently-labeled phospholipids in a fashion similar to, yet distinct from, single-celled eukaryotes and prokaryotes (Figure 6A). To assess the viability of the HEK cells immobilized via CDA, fluorescent probes were utilized. Live cells are distinguished by the presence of ubiquitous intracellular esterase activity, determined by the enzymatic conversion of the virtually nonfluorescent cell-permeant calcein AM to the fluorescent calcein, producing an intense uniform green fluorescence in live cells (Figure 6 A and B). Ethidium homodimer enters cells with damaged membranes and undergoes a 40-fold

enhancement of fluorescence upon binding to nucleic acids, thereby producing a bright red fluorescence in dead cells (Figure 6C). With the usual CDA protocol, we determined that the number of cells alive after one hour is at least equal to the number of cells alive in buffer, indicating that the CDA immobilization process does not cause irreversible damage to the cell. We will further investigate the ability to introduce minimal essential media during the immobilization process to extend the viability and functionality of mammalian cells immobilized using cell-directed assembly, allowing us to investigate many cellular processes including the onset of various diseases.

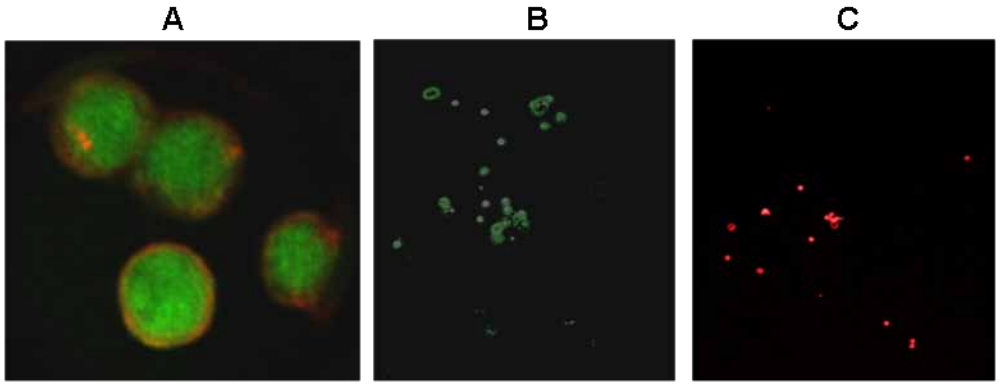

Figure 6. (A) HEK cells immobilized in a nanostructured silica film via CDA with fluorescent-green phospholipid. Cells are stained with a red fluorescent probe. (B) and (C) fluorescent images showing the viability of immobilized HEK cells with live cells appearing green and dead cells appearing red. Images are of the same field with colors separated for clarity in assessment.

2.5 Cellular Integration into pre-assembled lipid/silica mesophase films

This year we have confirmed our discovery of cellular integration into pre-formed lipid/silica mesosphase films (Figure 7) and have extended this approach to bacterial and mammalian cell lines. Remarkably cells introduced in water, buffer, or media onto an ordered lipid- or glycerol monoleate templated surface cause almost immediate rearrangement of the lipid/silica matrix to create a bio/nano interface quite similar to that formed by direct CDA. This approach has several advantages over CDA: 1) as drying and self-assembly of the lipid/silica mesophase film occurs prior to introduction of cells, the cells are not exposed to solvent and acid catalyst, and we expect any associated osmotic stress to be reduced. 2) this approach preserves the original nanoscale architecture directed by the chosen lipid template. 3) The approach is amenable to patterning using direct write procedures like ink-jet printing or selective wetting (see more in next section), which should allow us to pattern cellular arrays with differing cell densities and connectivities. Figure 7A below shows a schematic of the approach. Confocal imaging of the green labeled lipid introduced in the pre-made film indicates that after cellular integration the lipid envelops the cell (Figure 7B). Corresponding viability studies indicate that integrated yeast and bacterial cell lines have comparable viability as those introduced by direct CDA. The most fascinating discovery in this area is the preliminary result shown in Figure 7C of a mammalian (mouse) rat macrophage cell which has apparently integrated itself into a pre-made *di*C_6PC/silica mesophase film. This structure observed in SEM without fixation is stable upon evacuation and electron beam exposure.

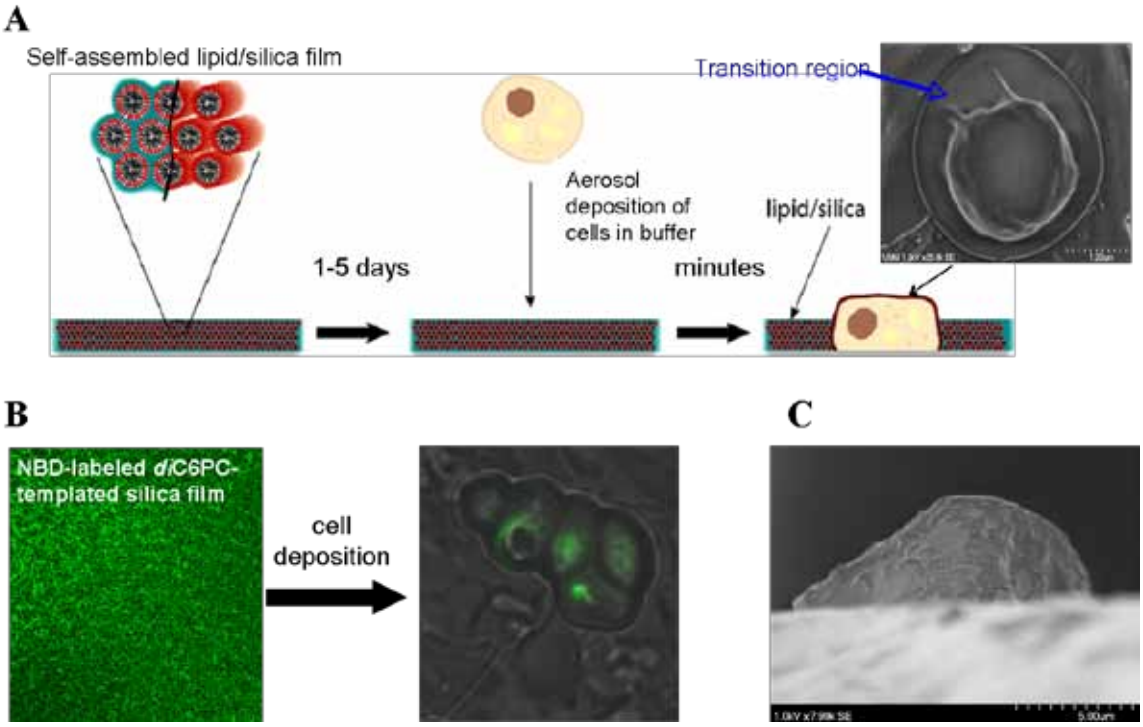

Figure 7. Cellular integration into pre-made *di*C_6PC/silica mesophase film. A) Schematic of process and SEM image of immobilized yeast cell, B) confocal microscopy of green labeled *di*C_6PC/silica pre-made film (left) and slice near top of integrated cell (right). C) SEM cross-sectional view of integrated mouse macrophage cell.

2.6 Selective wetting to pattern living cells into functional and connected arrays

In order to control the placement of cells and their spacio-temporal interactions, we have developed a novel optical patterning technique, which is not only simple and direct but also biologically compatible. Nanostructured silica films are created via evaporation induced self-assembly of aqueous silica precursors with a biologically compatible surfactant, glycerol monooleate (GMO) via dip-coating, spin-coating, drop-casting, or aerosol deposition. GISAXS studies show the films to form a highly ordered cubic mesostructure. The surfactant can be removed by calcinations or by UV/ozone lithography to yield a porous silica film.

To create patterned regions for cellular integration into the nanostructured silica matrix, we exploit the change in the hydrophobicity and fluidity of the surface of the film upon UV/ozone exposure. When the film is first deposited, it has a relatively low contact angle with water and remains in a semi-solid state. Upon exposure to UV/ozone, the GMO begins to photodecompose and the silanol precursors become more condensed. This yields a pattern where UV/ozone exposed regions are more hydrophobic and solidified and adjoining unexposed regions are more fluid and hydrophilic. Longer exposure to UV/ ozone removes the surfactant entirely, leaving a porous and extremely hydrophilic film surface. This trend

is shown below in Figure 8A. The use of a standard UV lithographic mask on top of the film allows for the definition of hydrophobic/hydrophilic regions when exposed to UV/ozone. The areas that are blocked by the mask remain hydrophilic, while exposed areas are more hydrophobic. Once these regions are defined, living cells introduced in water (or a water-based nutrient media) selectively localize to the defined hydrophilic regions. We have demonstrated this optically-controlled patterning method with many types of cells. Figure 8B shows an example with yeast cells, where the yeast is localized on the unexposed regions.

The functionality of this system has also been further extended using the ability to remove the surfactant to regain a hydrophilic film that is now porous. After deposition of the cells onto the hydrophilic/hydrophobic patterned film, the degraded surfactant in the hydrophobic portions can be completely removed using UV light and ozone, leaving porous, hydrophilic portions of the film. With the appropriate pattern on a UV mask, this technique can be used to create porous regions between the localized cells that can be used to introduce nutrient media, growth factors, toxins, or other molecules of interest, as shown below in Figure 8C. These techniques, when used in conjunction, form a new, simple yet powerful way to integrate traditional lithography with living cells.

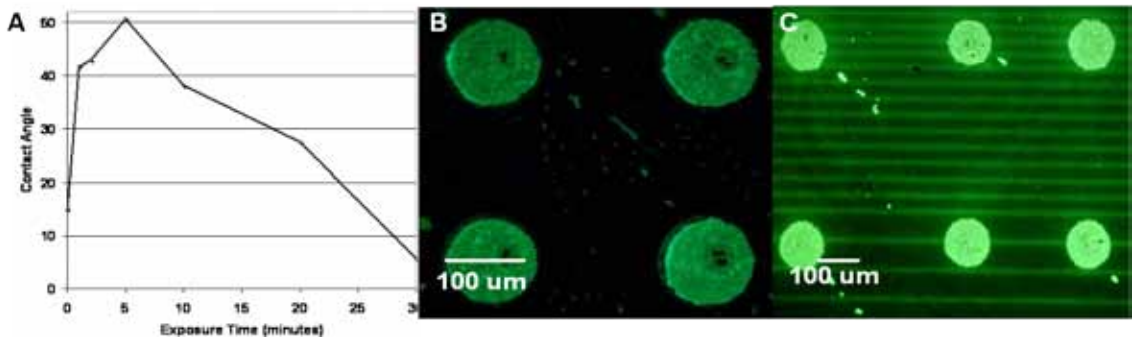

Figure 8. A) Water contact angle of a GMO-templated silica film as a function of UV light and ozone exposure time, B) Localization of fluorescently-tagged yeast onto the hydrophilic regions of an optically patterned nanostructured silica film, and C) Porous regions in connecting patches of cells have been created through further UV/ozone exposure and the resulting regions have been filled with a fluorescent nutrient media for visualization.

2.7 Develop a platform which utilizes CDA to interrogate cell communication at the single-cell level

Nearly all bacteria emit and sense small, diffusible 'signaling' molecules (autoinducers) whose extracellular concentration regulates gene expression through a positive feedback system, controlling important functions including virulence and biofilm formation[i]. The prevailing view of why this signaling takes place is that it allows populations of cells to assess their density i.e. to quorum sense (QS). If a quorum exists, bacteria coordinate their gene expression to function as a community, thereby providing group benefits exceeding those of individual cells[ii]. This idea that bacteria act cooperatively for the social

good is so appealing that the potential benefits of quorum sensing at the individual cell level have not yet been fully explored[iii,iv,v]. Here we developed a physical system that simulates endosomal or phagosomal bacterial entrapment during infection and maintains cell viability under conditions of complete chemical and physical isolation. For *Staphylococcus aureus*, we show quorum sensing and genetic re-programming to occur in a single organism. This 'discrete' quorum sensing allows *S. aureus* to sense confinement and to activate virulence and metabolic pathways needed for survival. To demonstrate the benefit of discrete quorum sensing to individuals, we showed quorum sensing bacteria to have significantly greater viability over non-QS bacteria. These data are consistent with evolutionary selection according to 'survival of the fittest' and imply that, for this medically important bacterial pathogen, QS contributes significantly to the survival of a single individual as well as to the entire population[vi].

Bacterial cells produce, secrete, detect and respond to small, hormone-like signaling molecules termed autoinducers[vii], - above a threshold extracellular concentration, bacteria alter gene expression, and therefore behavior. The QS hypothesis is that because the local autoinducer concentration can be cell density dependent, bacteria use signaling to monitor the environment for other bacteria. When a quorum is detected, genetic reprogramming occurs to coordinate cooperative behaviors at the population level, providing group benefits that would be unproductive at lower density[ii]. This interpretation of QS, however, ignores the cell's inability to distinguish between density and other factors influencing extracellular autoinducer concentration such as mass transport, confinement, and degradation, since a response is triggered only if the rates of autoinducer production, mass transfer and decay integrated over time reach a threshold concentration at the cell's location[iv]. This deficiency led Redfield[iii] to propose QS to be diffusion sensing, while Hense et al.[iv] proposed the term efficiency sensing: autoinducers would be used as metabolically cheap trial balloons to estimate the value to the group of producing more costly, extracellular products. These alternative QS motives depend strictly on local autoinducer concentration and should operate at the individual organism level. This is important, because complex group behaviors need to be invoked to account for both QS evolution and maintenance as 'cheating' can be common, and evolutionary theory predicts that individuals who communicate and cooperate can be exploited by those who do not[5,ii]. To reconcile these different perspectives, we hypothesized that QS, independent of any group benefit (which may be significant), must operate at the single cell level to provide fitness benefits to individual bacteria that can be selected for evolutionarily. To verify this hypothesis, we developed a physical system to isolate individual *S. aureus* and examined confinement-induced effects on signaling, gene expression, and viability. Here we show self-induction and resultant genetic reprogramming to occur efficiently in individual organisms.

S. aureus is primarily a commensal that resides in a nonpathogenic state. It detects and responds to an extracellular autoinducer peptide (AIP)[7]. Above a threshold AIP concentration, a QS cascade is activated causing down-regulation of adhesins and up-regulation of an array of toxins, hemolysins, degradatory enzymes, and metabolic pathways. Micro-array studies have revealed that 104 genes are up-regulated and 34 are down-regulated, representing ~5% of the genome[viii]. In *S. aureus*, the accessory gene regulator *agr* operon is responsible for QS regulation. It contains two divergent transcripts, RNAII and RNAIII. RNAII encodes four genes, *agrBDCA*, that are required to synthesize, export, and detect AIP. AgrC and AgrA form a two-component regulatory pair - AIP binding to its surface receptor, AgrC, activates a phosphorylation cascade. When phosphorylated, AgrA binds and induces expression of RNAIII, which encodes a regulatory RNA that represses adhesin expression and induces production of secreted virulence and degradatory factors. AgrA-P also induces expression of the RNAII transcript, exerting positive feedback control on this regulatory system[ix].

To date, quorum sensing in *S. aureus* has been studied exclusively with large numbers of bacteria (1×10^7-1×10^9) in either broth suspension cultures or cell cultures of phagocytosed bacteria. Therefore, the potential for individual staphylococci to autoinduce in the absence of neighboring bacteria or cell signaling interference inherent in these systems is currently unknown. To observe QS in isolated, individual cells, *S. aureus* were immobilized, individually (or in small groups, see Fig. 5), within a matrix fabricated at a sufficiently small physical scale (~20 µm diameter, physically isolated hemispherical droplets, see Fig. 1A and B) so that the overall cell density (~1 cell per 4×10^3 µm^3, equivalent to ~0.5×10^9 cells ml^{-1}) exceeded the reported QS threshold ($10^7 - 10^9$ cells ml^{-1}). The matrix was formed by adaptation of our cell-directed assembly approach[x] to an aerosol procedure we developed previously to form ordered porous silica nanospheres[xi]. It results in cells incorporated within a lipid vesicle maintained at physiological pH surrounded by an ordered silicon dioxide nanostructure (Fig. 1) that serves as a reservoir for buffer and media. This construct mimics a bacterium entrapped in an intracellular membrane-bound compartment (endosome or phagosome) that establishes the effective cell density (>> QS threshold) and the relevant volume in which AIP can accumulate to trigger a response. Importantly, this architecture allows individual cells to be maintained in a viable state under externally dry conditions[xii] that establish complete physical and chemical isolation of one cell from all others. This reduced physical system is biologically relevant, because *Staphylococcus aureus* is known to become trapped in such intracellular compartments, and it is proposed that they employ a QS strategy to induce new gene expression, promoting intracellular survival and/or escape[xiii].

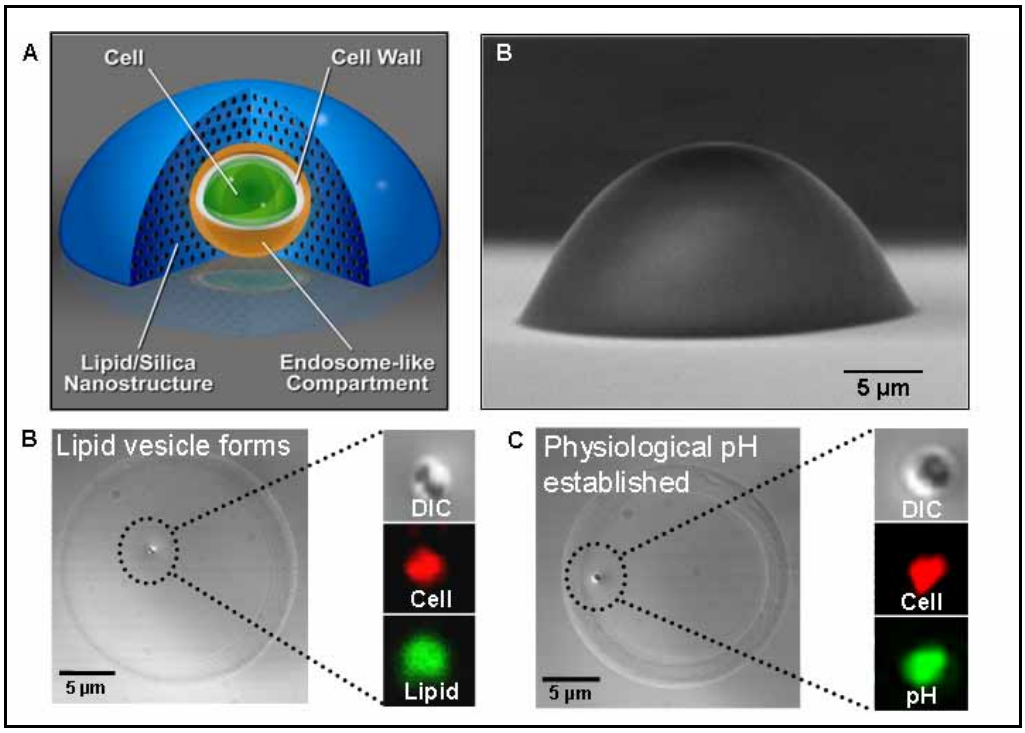

Figure 4. Isolation of individual *S. aureus* within a nanostructured droplet. (**A**) schematic of physical system (not to scale) showing a cell incorporated in an endosome-like lipid vesicle within a surrounding nanostructured lipid/silica droplet deposited on glass substrate and (**B**) SEM image of physical system. The nanostructure maintains cell viability under dry external conditions and allows complete chemical and physical isolation of one cell from all others. **C** and **D** show plan-view optical microscope images of individual cells in droplets (large outer circular areas). Magnified areas show differential interference contrast image and red fluorescence image of individual stained, isolated cells (both **C** and **D**) and green fluorescence image of NBD-labeled lipid localization at cell surface

(**C**) or localized pH (**D**, using Oregon Green pH-sensitive dye). We find that, within the droplet, the cells become enveloped in an endosome-like lipid vesicle (**C**), and establish a localized pH consistent with physiological endosomal conditions (**D**). For further information regarding aerosol assisted droplet formation and lipid localization and pH establishment, see references 11 and 12.

To optically monitor the onset and kinetics of auto-induced QS, we used *S. aureus* strains ALC1743 (*agr* group 1 RN6390 containing reporter *agr*: P3-gfp) and ALC1740 (RN6390 containing reporter *hla*-gfp) at an early exponential phase prior to QS induction. Expression of green fluorescent protein (GFP) by ALC1743 reports late exponential phase-dependent activation of QS, while in ALC1740 it reports QS-mediated downstream synthesis of the pore-forming toxin, a-hemolysin. Figure 2 shows GFP expression over time for isolated, individual *S. aureus* strain ALC1743 and representative confocal images of isolated, red-stained ALC1743 immediately following encapsulation and after ten hours of incubation at 37˚C. GFP expression was detected at 2 hours, and it increased progressively with time, exceeding 90% at ten hours. (Equivalent QS activation was also obtained for the Newman strain containing reporter *agr*.P3-*gfp*).

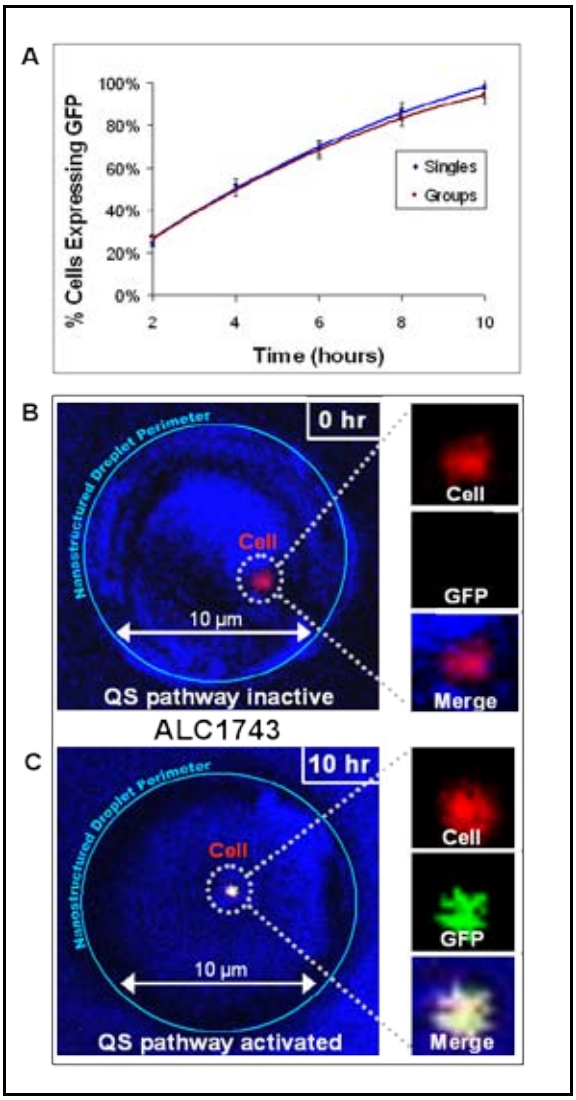

Figure 5. Auto-induction of S. aureus strain ALC1743. (**A**) Percentage of individual cells (or small groups of cells) expressing GFP as function of incubation time at 37°C. (**B**, **C**) Representative confocal images of GFP expression of red stained S. aureus. Both main images show the merged confocal fluorescence image of a S. aureus ALC1743 cell (stained red) within a nanostructured droplet (pseudo-colored blue). Enlarged images show discrete fluorescence channels for the red cell stain, green fluorescent protein production, and a merged image for confirming co-localization of any GFP production by the cell. Initially, the absence of GFP production by individual cells indicates the QS pathway is inactive (**B**). However, after ten hours, GFP expression can be observed in individual cells, indicating that the initial stage of the QS pathway has been activated (**C**).

Figure 3 shows corresponding, representative confocal images of isolated, individual *S. aureus* strain ALC1740 after zero and ten hours of incubation. Strong GFP expression after ten hours shows activation of the RNAIII-promoted pathway that induces expression of secreted virulence factors. Here we specifically detect activation of the a-hemolysin promoter. Together Figures 2 and 3 provide the first proof of auto-induction of individual *S. aureus*. This 'discrete' quorum sensing allows *S. aureus* to sense confinement through increased extracellular concentration of autoinducer and to activate virulence factor pathways and initiate new gene expression needed to survive in such confined environments. Importantly,

the kinetics of GFP induction was equivalent for small clusters of confined bacteria as well as individuals (Fig. 2C) indicating that QS occurs at the individual level whether as singles or groups of bacteria.

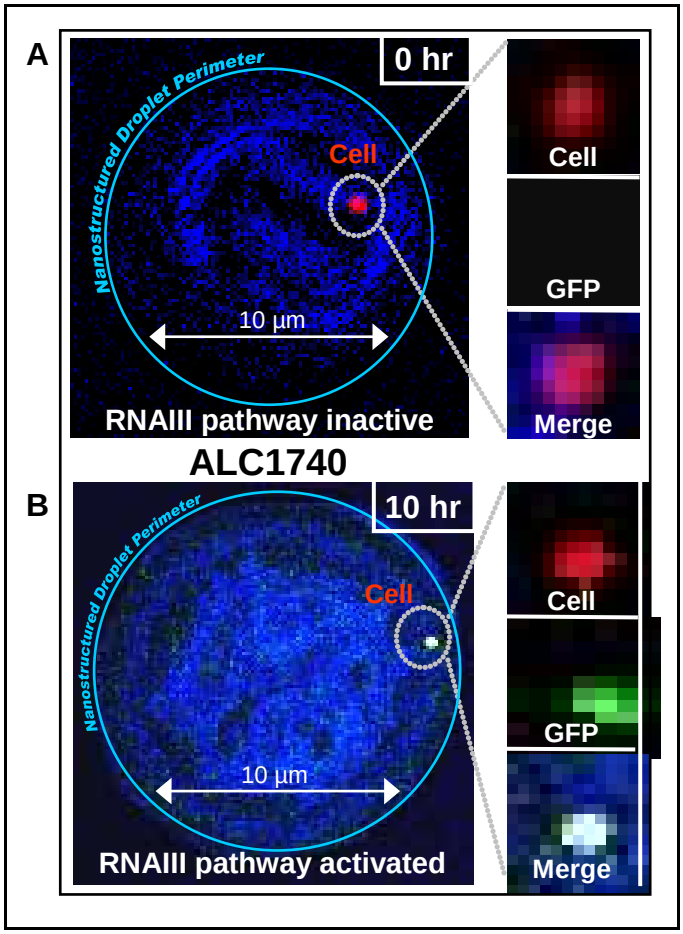

Figure 6. Representative confocal images of GFP expression of red stained *S. aureus* strain ALC1740. (**A**, **B**) Both main images show the merged confocal fluorescence image of a *S. aureus* ALC1740 cell (stained red) within a nanostructured droplet (pseudo-colored blue). Enlarged images show discrete fluorescence channels for the red cell stain, green fluorescent protein production, and a merged image for confirming co-localization of any GFP production by the cell. Initially, the absence of GFP production by individual cells indicates the toxin, α-hemolysin, is not being produced (**A**). However, after ten hours of incubation in air at 37ºC, GFP expression can be observed in individual cells showing activation of the RNAIII-promoted pathway that induces expression of secreted virulence factors (**B**). Here we specifically detect activation of the a-hemolysin promoter.

To demonstrate the benefit of discrete quorum sensing to individuals, we compared the viability of isolated, individual RN6390 to that of RN6911, a RN6390 mutant unable to initiate QS due to deletion of the *agr* operon. Figure 4 shows that, over an 18-day incubation period confined within the media-enriched silica matrix at 37°C, the viability of RN6390 (*agr*+) was significantly greater than that of the isolated mutant RN6911 (*agr*-) (P = 0.046, Gehan-Breslow survival analysis, compare Fig. 4 plots A and B). A

plausible explanation for the viability difference is that confinement-induced QS and attendant up-regulation of a spectrum of genes affecting virulence and metabolism enhances utilization of external nutrients. Consistent with this idea, the viability of *agr*+ isolated in a matrix without nutrients (Fig. 4 plot C) was statistically equivalent to that of the *agr*- mutant isolated in a nutrient containing matrix (Fig. 4 plot B) and the additional control, *agr*-, immobilized within a matrix fabricated without nutrients (Fig. 4, plot D). These data suggest an alternative motive for QS where discrete quorum sensing and genetic re-programming provide benefits to enable survival of individuals.

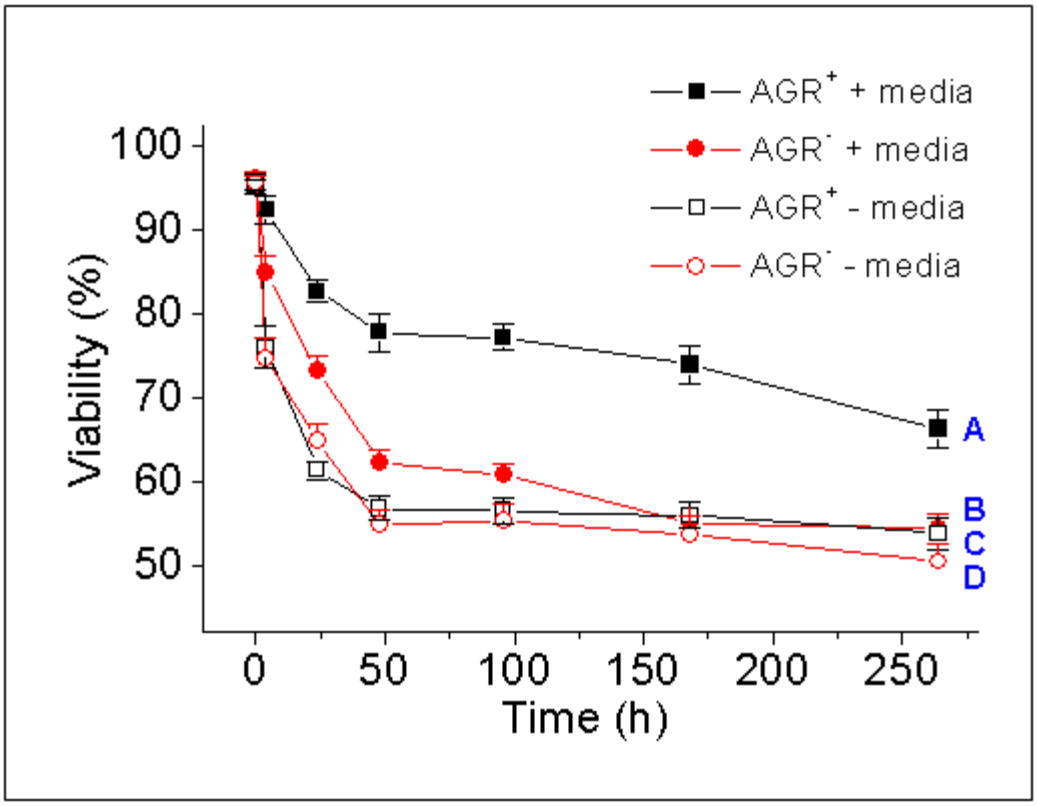

Figure 7. Viability of *agr*+ and *agr*- strains of individual *S. aureus* cells isolated within nanostructured lipid/silica droplets (**A**) RN6390 (*agr*+) in droplet containing media, (**B**) RN6911 (*agr*-) in droplet containing media, (**C**) RN6390 (*agr*+) in droplet without media, (**D**) RN6911 (*agr*-) in droplet without media. Viability determined using BacLight fluorescent viability probe kit.

By use of a reduced physical system, devoid of inter-cellular signaling interference inherent to bulk cultures[xiv,xv] and previous studies of endosomal entrapment [xii,xvi] we demonstrated confinement-induced quorum sensing for an individual organism. Isolated *S. aureus* senses confinement through accumulation of AIP and activation of the two-component response regulatory system with its inherent positive-feedback control. Up-regulation of the *agr* effector molecule RNAIII enhances the expression of a diverse array of genes associated with metabolism, transport, and virulence. As shown by viability studies, benefit to the individual is conferred by poising the cell to be able to scavenge for nutrients and thus better

survive in isolation. We envision this 'discrete' quorum sensing and its resultant fitness benefits to the individual to be general. It provides an alternative model for QS that does not require complex social interactions for its evolution or maintenance, but rather promotes evolutionary selection according to survival of the fittest individuals.

METHODS AND MATERIALS

The *Staphylococcus aureus* strains used in this study, ALC1743 (*agr* group 1 RN6390 containing reporter *agr*: P3-gfp), ALC1740 (RN6390 containing reporter *hla*-gfp), wild-type Newman containing reporter *agr*.P3-*gfp*, wild-type RN6390, and RN6911 (RN6390 *agr* deletion mutant) were generated and grown in TSB broth to early exponential phase before freezing in stock[xvii].

Isolated nanostructured droplets containing individual cells (or small groups of cells, see e.g. Fig. 1) were prepared by an extension of our evaporation-induced self-assembly process where an amphiphilic short chain phospholipid was used as a biocompatible surfactant[x,xi]. Upon evaporation, lipids direct the organization of silica into an ordered lipid/silica nanostructure, which serves in our experiment as a synthetic intracellular milieu in which to incorporate individual cells. To prepare these droplets, stock solutions of soluble silica precursors were prepared by refluxing tetraethylorthosilicate (TEOS), ethanol, de-ionized water and HCl (molar ratios 1: 4: 1: 5x10-5) for 90 minutes at 60ºC. Water, HCl and trypticase soy broth (TSB) (a media serving as a nutrient required for GFP expression) were added to the stock solution to achieve a biologically compatible sol with final molar ratios of 1 TEOS: 4 ethanol: 0.01 HCl: 6 water: 6 TSB. 30 mg/mL of the C6 phospholipid, dihexanoylphosphatidylcholine (Avanti Polar Lipids), was then added to the silica solution. ALC1743 and ALC1740 (not expressing GFP) were centrifuged and immediately resuspended/diluted in water. These cells were added to the silica/lipid solution to yield a final concentration of 10^6 cells/ml << quorum sensing threshold. The sol was immediately aerosol deposited onto glass resulting in physically and chemically isolated (approximately) hemispherical droplets (Figure 5, A) containing individual or small groups of cells as determined by confocal microscopy (see below). The silica matrix is characterized by a periodic uniform lipid/silica nanostructure as confirmed by small angle x-ray scattering (Fig. 5, B). Encapsulated cells prepared with either optically labeled lipid (NBD) or a fluorescent pH probe (Oregon Green) allowed visualization of lipid localization around the cell or maintenance of a localized physiologically buffered pH (Fig. 5, I, J), similar to that reported previously for our cell-directed assembly process[ix]. Individual cell-containing droplets are maintained in air and separated by air gaps with spacings comparable to or exceeding the droplet diameters (10-20 μm), preventing any AIP diffusion between droplets during experiments.

Following deposition, droplets were incubated at 37ºC for indicated periods of time in air (nanostructure maintains and supplies water and nutrients). Additional samples were also refrigerated for identical periods of time and used to verify the absence of GFP expression in cell stocks. After incubation, samples were stained with SYTO 64 for visualization, washed, fixed, and mounted using DABCO anti-fade reagent. (Due to rapid photobleaching of individual cells, it was not possible to monitor GFP induction in real time using fluorescence microscopy. Therefore fixation and mounting with anti-fade was necessary for confocal imaging). Samples were then imaged on a Zeiss LSM 510-META confocal system mounted on a Zeiss Axiovert 100 inverted microscope. Fluorescence emission fingerprinting followed by linear unmixing via integrated software was used to separate the fluors from the autofluorescence of the nanostructured silica matrix and confirm the presence of GFP in the cells (Fig. 5, C-H).

To evaluate the viability of individual cells encapsulated in the nanostructured droplets, *S. aureus* strains RN6930 and RN6911 were immobilized as described above. The cells in droplets were then incubated in air at 37ºC for the indicated periods of time. At the indicated intervals, samples were removed from the incubator and evaluated using the Baclight (Invitrogen) viability dye set using a standard protocol to allow labeling and imaging of immobilized cells. Viability was then determined using a Nikon TE2000 inverted fluorescence microscope equipped with a viability dye filter set from Chroma. Each point represents average of nine determinations of approximately one hundred cells each.

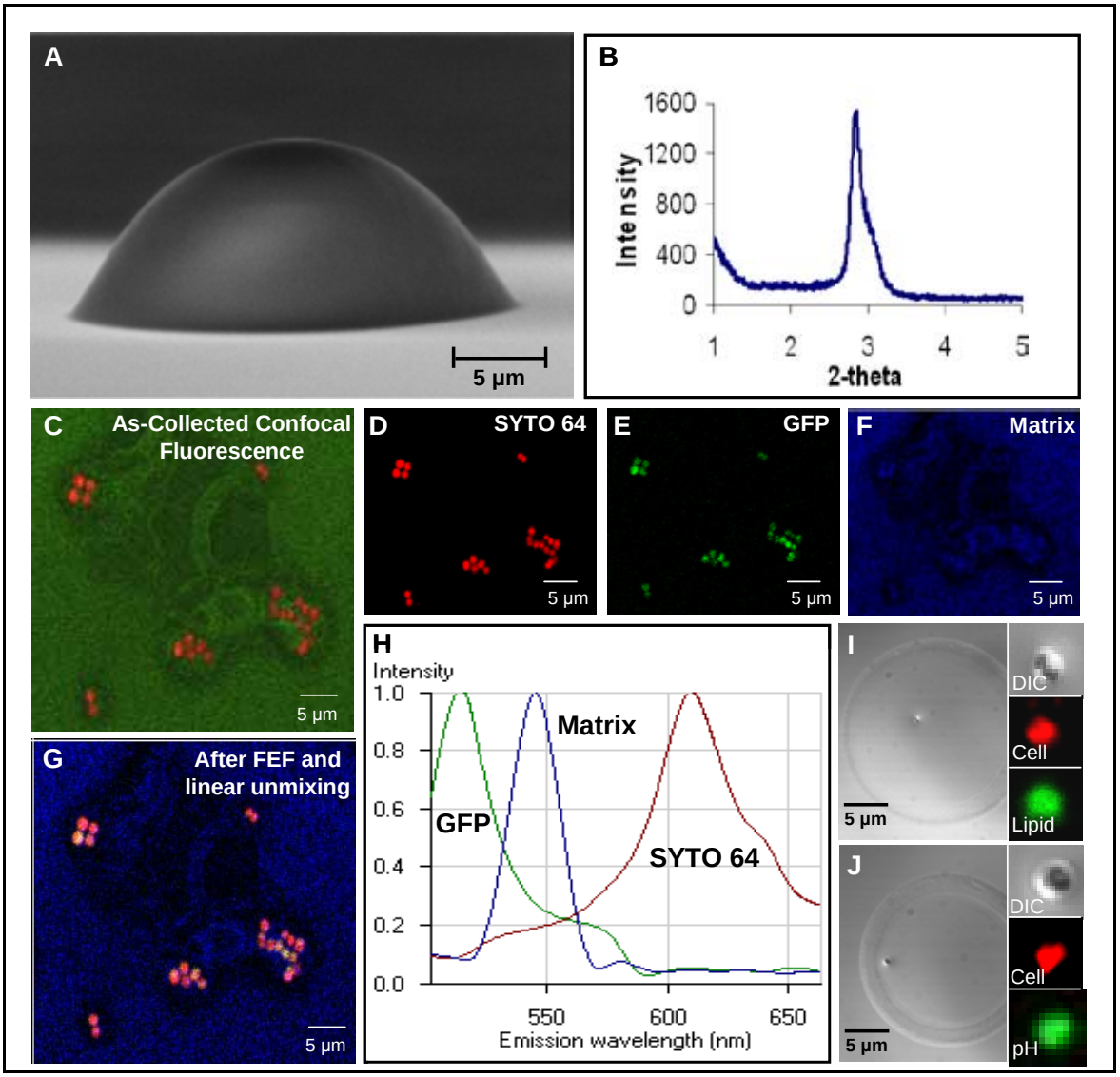

Figure 8. S. aureus cells expressing GFP were stained with SYTO 64 and immobilized in a nanostructured silica matrix. An SEM micrograph shows the general size and shape of the matrix droplets (**A**), while x-ray diffraction was used to confirm the presence of an ordered nanostructure within the matrix (**B**). The silica matrix displays a large amount of autofluorescence (green), making resolution of the colocalization of GFP (green) and cell stain (red)

difficult using standard confocal fluorescent microscopy (**C**). Following isolation of relevant spectra using control samples (**H**), fluorescence emission fingerprinting - FEF - can be used to obtain linear unmixed channels for the red cell stain SYTO 64 (**D**), GFP (**E**), and the silica matrix (**F**, pseudo-colored blue for clarity). The unmixed channels can then be merged as in traditional fluorescence microscopy (**G**). Confocal fluorescence images of NBD-tagged lipid localized around a cell in a droplet (**I**) and a buffered pH region near a cell visualized with a pH indicator that fluoresces at neutral pH (**J**) were used to establish the physical characteristics of this system to be similar to those of our previously reported cell-directed assembly process[x]. All inset images are shown at an additional 5x magnification for clarity.

2.8 Expand our lithography-with-life approach to include functional mammalian cells

One major limitation of our well-studied cell-directed assembly process is the inability to successfully immobilize mammalian cells with retained functionality. The benefits of CDA are not seen with mammalian cells because the exposure to solvent and drying stresses involved in traditional CDA can not be mediated by mammalian cells due to their lack of a cell wall. The cell-directed integration process seeks to minimize cell exposure to these stresses and therefore should be more compatible with mammalian cells.

To investigate the ability to immobilize mammalian cells using CDI, a genetically-modified mouse macrophage (RAW 264.7 Murine Macrophage - available through a collaboration with Sandia National Laboratories) was chosen to allow for simultaneous assessment of viability, accessibility, and functionality. The cells contain a GFP-fusion protein which will undergo ATP-dependent translocation into the cytosol during activation of the toll-like receptor 4 signal pathway by a model antigen, lipopolysaccharide (LPS), as shown below in Figure 9. Once these cells have been integrated, LPS can be introduced. If translocation of the GFP is observed, then accessibility of the cells to the surrounding external environment, functionality of cell surface proteins, and ability to conduct normal metabolic process are all confirmed.

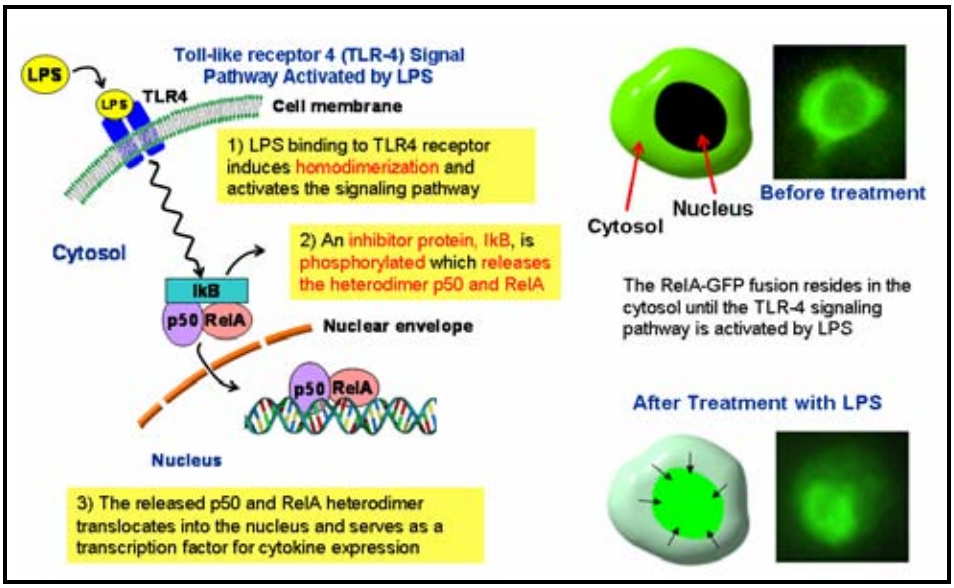

Figure 9. Genetic modification of macrophages for verification of accessibility, surface functionality, and viability. In this system, a GFP-fusion protein resides normally in the cytosol of the cell. However, in the presence of the model endotoxin lipopolysaccharide (LPS) and media, an ATP-dependent translocation of the fusion protein to the nucleus is observed.

To prepare macrophages for integration, the cells were removed from their culture dish using trypsin and resuspended in PBS. Nanostructured silica films containing *di*C_6PC were created as for the bacterial cells and yeast integrations. Macrophages in buffer were then added to the film using a pipette and allowed to integrate at room temperature for 2 minutes. Following washing of films with excess buffer, films were visualized using fluorescence microscopy to verify the presence of cells, as shown below in Figure 10. It can be seen that many cells remain on the film after washing, indicating the possibility of mammalian cell integration.

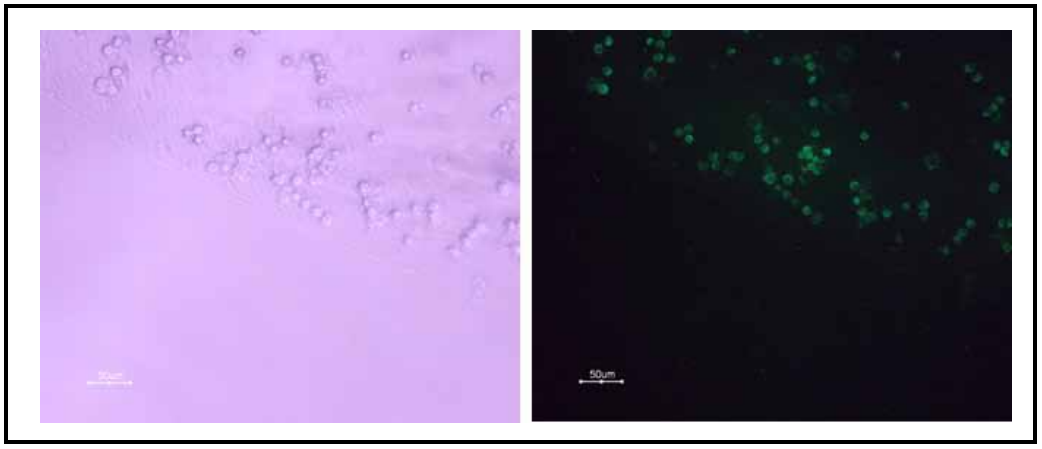

Figure 10. Optical and fluorescence images of macrophages integrated into a *di*C_6PC/silica film. Phase contrast (left) and fluorescence images (right) of the edge of a droplet of concentrated GFP-modified macrophages which have integrated at room temperature for 20 minutes.

To judge immediate interactions of the cells with the material, green fluorescently-labeled lipid was used to prepare additional *di*C_6PC/silica nanostructured films. Again, macrophages were added in buffer and allowed to incubate for two minutes prior to washing. As can be seen in Figure 11, the green lipid is redistributed in the area containing the cells. Although exact determination of lipid localization is difficult due to the ubiquitous presence of GFP in the cells, it can clearly be seen that the cells have some interaction with the film resulting in reorganization of the lipid, indicating that the cells are not simply sitting on top of the film. This is the same observation made with the yeast and the bacterial cells, indicating the localization of lipid around the cells.

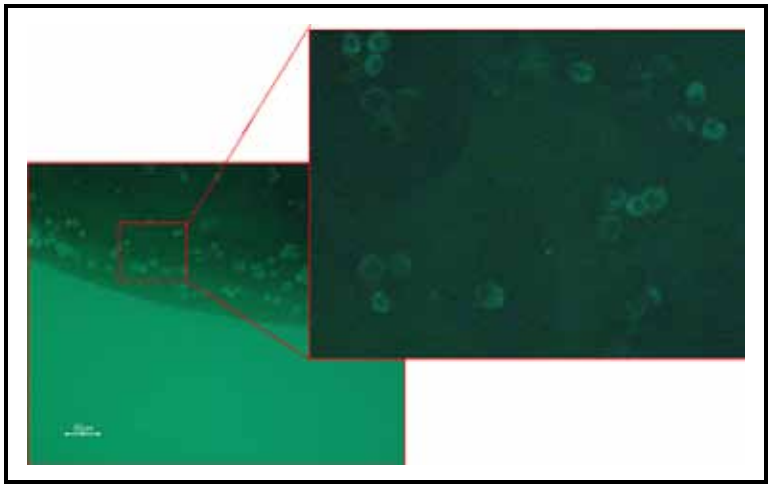

Figure 11. Fluorescence image of lipid reorganization by microphages in an NBD *di*C_6PC/silica film. (Left) Redistribution of the lipid in the film (bright green) can be seen in a droplet of live GFP-modified macrophages (dull green). (Right) Higher magnification shows local regions of lipid reorganization around various groups of cells.

Verification of full-cell integration was then performed using SEM and EDS as for the yeast and bacteria. It is found that the macrophages can readily be imaged under the high-voltage electron beam after being allowed to incubate on the *di*C_6PC/silica films, indicating that the cells are protected by an insulating layer of silica as shown below in Figure 12. Again a transition region can be observed extending from the bulk film to the cell surface. However, this region appears much smaller due to the much larger size of the macrophage cells compared to the yeast and bacterial cells.

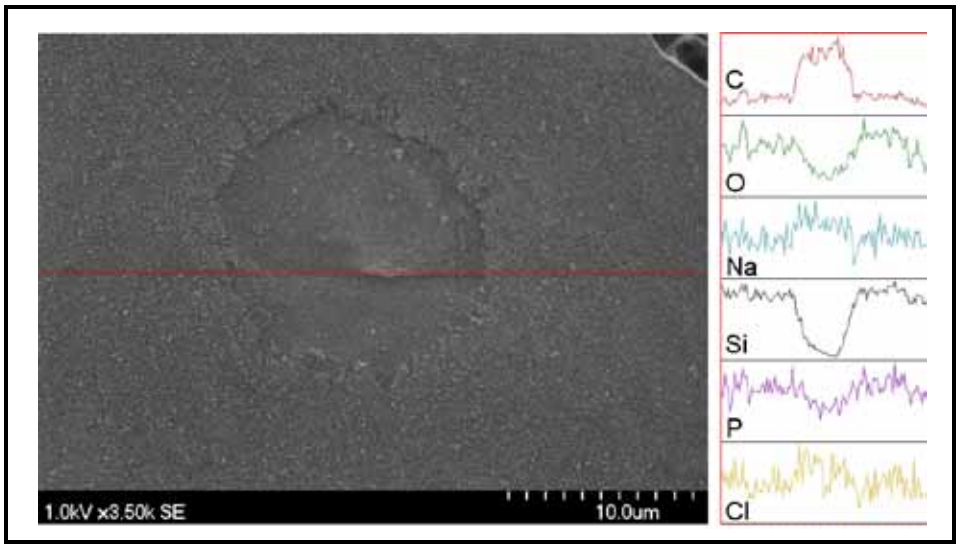

Figure 12. SEM image with corresponding EDS line scan of an integrated macrophage cell. SEM (left) of yeast show a region of transient elemental composition in the local vicinity of the cell as indicated by an EDS line scan (red).

Full, three-dimensional integration and encapsulation of the macrophage cells was then confirmed using cross-sectional SEM along with spotlight EDS and spectral elemental verification, as shown below in Figure 13. It is seen that cell retains a familiar 3D appearance. In addition to the ability to directly visualize these cells without any preliminary preparation, full encapsulation was confirmed by the spectral elemental analysis identifying the presence of silica on the top of the cell. Collectively, this data indicates that the cell-directed integration process can be used to immobilize and encapsulate mammalian cells in a manner similar to yeast and bacteria encapsulation.

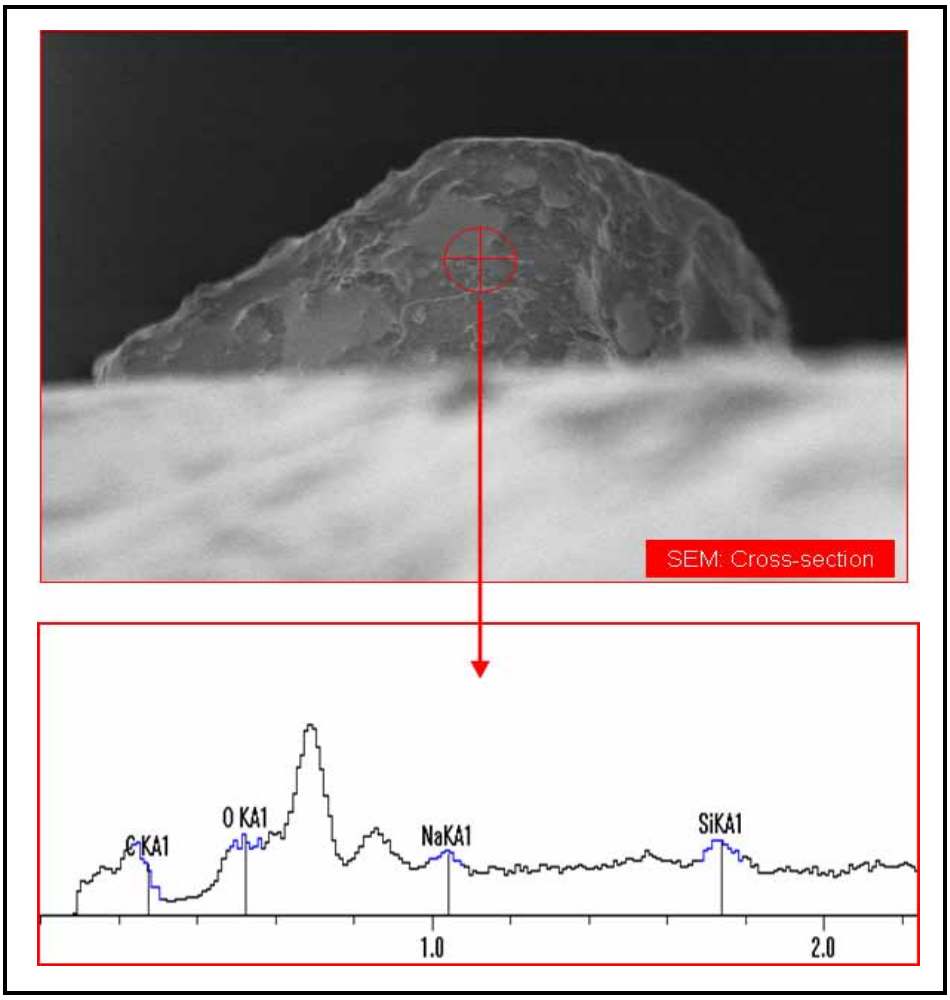

Figure 13. SEM cross-section and EDS spotlight confirm full integration of macrophages via CDI. (Top) SEM cross-sectional image of integrated macrophage. Spotlight (red) indicates area where EDS elemental confirmation was collected (bottom). It can be seen that the presence of silica around the cell is confirmed by automatic elemental recognition (blue).

Once the integration of the macrophages was confirmed, viability was assessed by way of the genetic modifications described above. Macrophage cells were integrated into nanostructured *di*C_6PC/silica films as previously discussed. After washing, films were dried and imaged using confocal microscopy to ensure that the integration process did not trigger non-specific translocation of the GFP-fusion protein. This data is shown below in Figure 14. After verifying that the integration process did not stimulate an immune response, the integrated cells were allowed to incubate in air at approximately 37ºC for 24 hours (actually they sat in my car in the summer). The cells were then incubated at 37ºC for 45 minutes in media containing 10 mM LPS. Films containing cells were then washed and imaged using confocal microscopy.

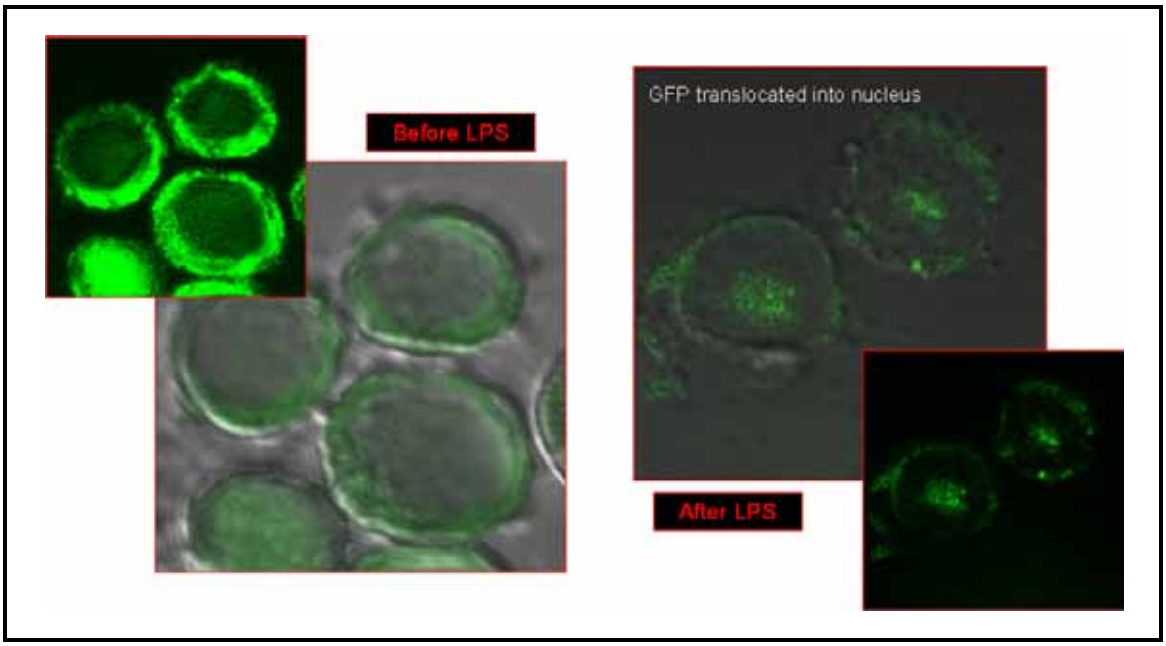

Figure 14. Confocal images confirming accessibility and functionality of integrated macrophages. (Left) Confocal and DIC images of macrophages following integration into a *di*C_6PC/silica film show the expected presence of the GFP-fusion protein in the cytosol of the cell, indicating that the integration process does not illicit an immune response. After incubating in air at 37ºC for 24 hours, LPS in media is added to the immobilized cells. (Right) Following incubation with LPS and media for 30 minutes at 37ºC, immobilized cells show translocation of GFP-fusion protein, confirming viability of the cells, as well as functionality of the cell surface receptors and accessibility of the cell to molecules of LPS and media.

Translocation of GFP to the nucleus can clearly be observed. Presence of GFP in the nucleus, as opposed to the top or bottom of the cell, was also confirmed through the use of confocal optical sectioning. This clearly shows that the integrated cells have remained viable for a much longer time than the cells normally survive even in buffer, where unintegrated cells survive for no more than 3 hours. From this data, we find that mammalian cells can be successfully immobilized using cell-directed integration. Using CDI with mammalian cells results in cells that are fully encapsulated in a nanostructured lipid/silica matrix while remaining accessible to the environment, allowing addition of nutrients and other molecules of interest. This indicates that cell-directed integration provides the world's first technique for encapsulation of live mammalian cells for use in solid-state cell-based devices and cell interrogation platforms.

2.9 Understand the mechanisms controlling integration of cells into self-assembled nanostructures

As with cell-directed assembly, the integration of living cells into pre-formed silica nanostructures in understandably complex. To investigate the influence of both the cells and the nanostructures on the integration process, a standard integration protocol and method for counting the number of cells needed to be developed. To begin, a *di*C_6PC/silica film was created using the standard spincoating procedure and allowed to condense. Then 1 µL of live, stationary-phase yeast cells in DI water at a concentration of $9*10^9$ cells/mL, stained with a red-fluorescent marker for easier visualization and counting, were allowed to integrate into the film at ambient conditions for various amounts of time, as shown in Figure 15. Following the interaction time, unintegrated cells were removed via washing for 10 seconds. Integration was then confirmed by SEM, EDS, and confocal microscopy as described above. Spots containing integrated cells were visualized using fluorescence microscopy and cells were counted using NIS-Elements microscopy imaging software.

We find that the number of cells that are able to integrate increases linearly for the first 30 minutes. After that time, a saturation level is reached. For this standard protocol, we achieve integration of approximately 1 in 6 cells. This number is likely to be limited by interactions between the cells and silica film relating to the contact angle and subsequent surface area for integration as well as the flocculation of the yeast. These results indicate that the integration process proceeds at a time scale that is similar to the initial silica condensation time, indicating that silica is re-hydrolyzed resulting in the fluidity of the silica during cell integration.

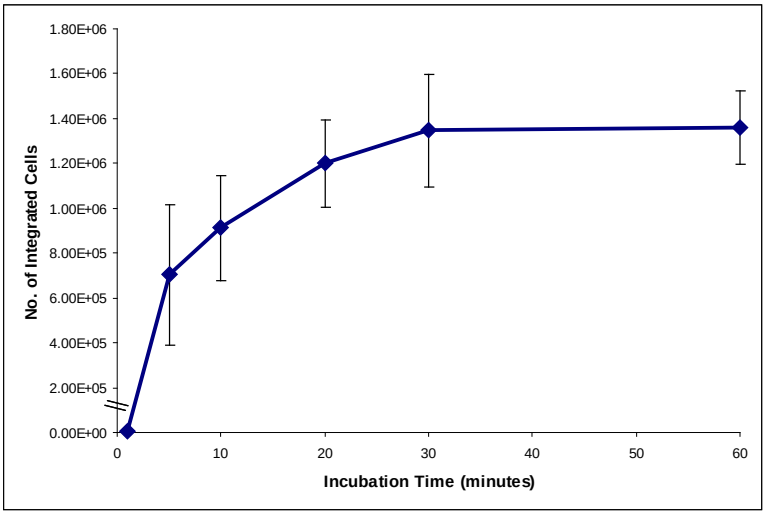

Figure 15. Number of integrated cells vs. incubation time. Approximately 10^7 yeast cells stained with SYTO 64 were added in water to premade *di*C_6PC/silica films and allowed to integrate for the indicated period of time at ambient conditions, after which unintegrated cells were washed off. The number of integrated cells was then counted using NIS-elements microscopy software. At all time points, n= 12. Error bars represent 95% confidence interval.

In order to establish this standard integration protocol, it was essential to ensure that the wash process was sufficient to remove all cells that were not integrated to obtain realistic and reliable data. We see in Figure 16 that the amount of cells present on a film decreases sharply with washing until a 10 second wash has been performed. After 10 seconds of washing, the number of cells on the film remains constant, indicating that all unintegrated cells have been removed.

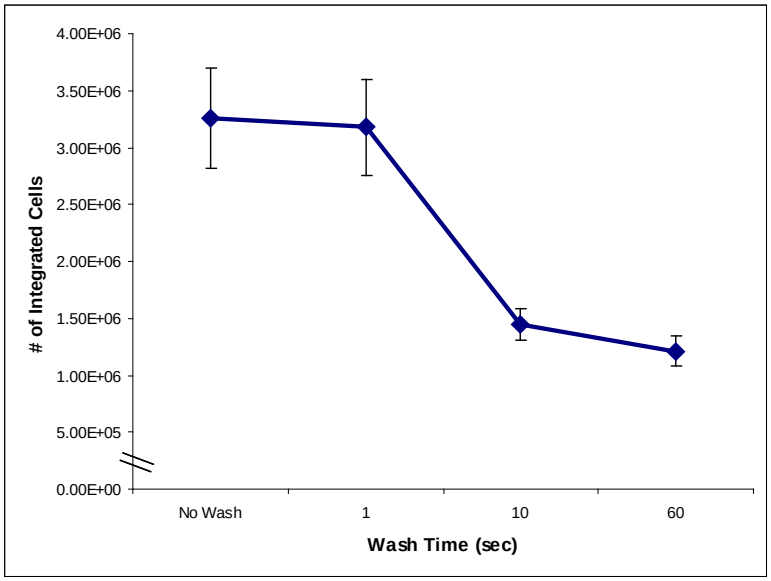

Figure 16. Number of cells on nanostructured silica film vs. wash time. Approximately 10^7 yeast cells stained with SYTO 64 were added in water to premade *di*C_6PC/silica films and allowed to integrate for 30 minutes at ambient conditions, after which unintegrated cells were removed by rinsing for the indicated period of time. The number of integrated cells was then counted using NIS-elements microscopy software. At all time points, n= 12. Error bars represent 95% confidence interval.

Assuming that intimate contact between the cells and lipid/silica film is required for integration, the competing effect of cell-cell contact may hinder cell integration. To investigate the effects of cell flocculation on the integration process, different initial concentrations of cells were allowed to integrate into a *di*C_6PC/silica film following the standard procedure developed above. From this data, shown below in Figure 17, we find that the number of cells that are able to integrate increases linearly over a physiologically relevant range of concentrations, indicating that cell-cell interactions are not substantially hindering cell-material interactions and integration. However, as the density of the cells increases, we begin to approach a limiting number of integrated cells. At these high densities, flocculation and subsequent stacking of cells prevents interaction of some cells with the film. These cells are not able to integrate and thus removed by washing, confirming the necessity of intimate cell-material contact for integration.

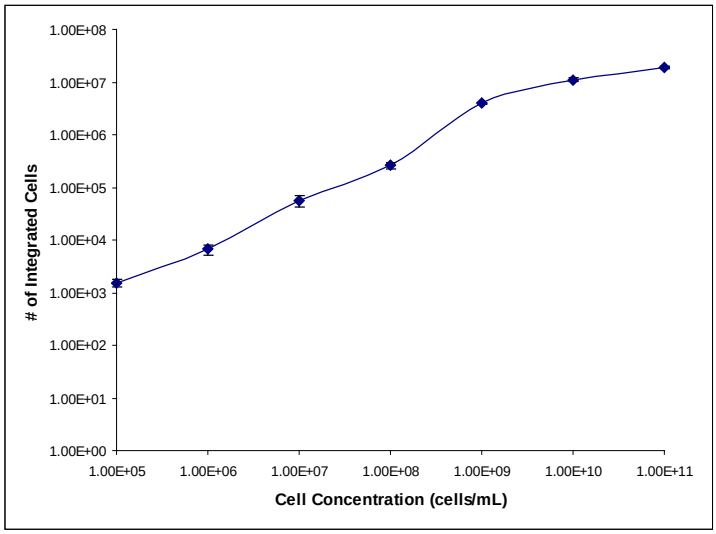

Figure 17. Number of integrated cells is linearly proportional to initial cell concentration over physiological values. Various concentrations of yeast cells stained with SYTO 64 were added in water to premade *di*C_6PC/silica films and allowed to integrate for 30 minutes at ambient conditions, after which unintegrated cells were removed by rinsing for 10 seconds. The number of integrated cells was then counted using NIS-elements microscopy software. At all time points, n= 12. Error bars represent 95% confidence interval.

Because of the observed similarities between integrated cells and cells immobilized using cell-directed assembly, it was assumed that cell-directed integration would also be a complex, active process requiring live cells. It has already been shown above that cell surrogates do not interact with the lipid or the silica and are not able to establish any pH gradients. Cell surrogates should, therefore, be unable to integrate themselves into a nanostructured silica film. To confirm this idea, latex bead cell surrogates were introduced to *di*C_6PC/silica films and counted as per the protocol developed for yeast above. As seen below in Figure 18, neither uncharged latex beads nor beads possessing a surface charge were retained after washing. This is a clear confirmation of the necessity of active interactions between live cells and the lipid/silica host to obtain integration.

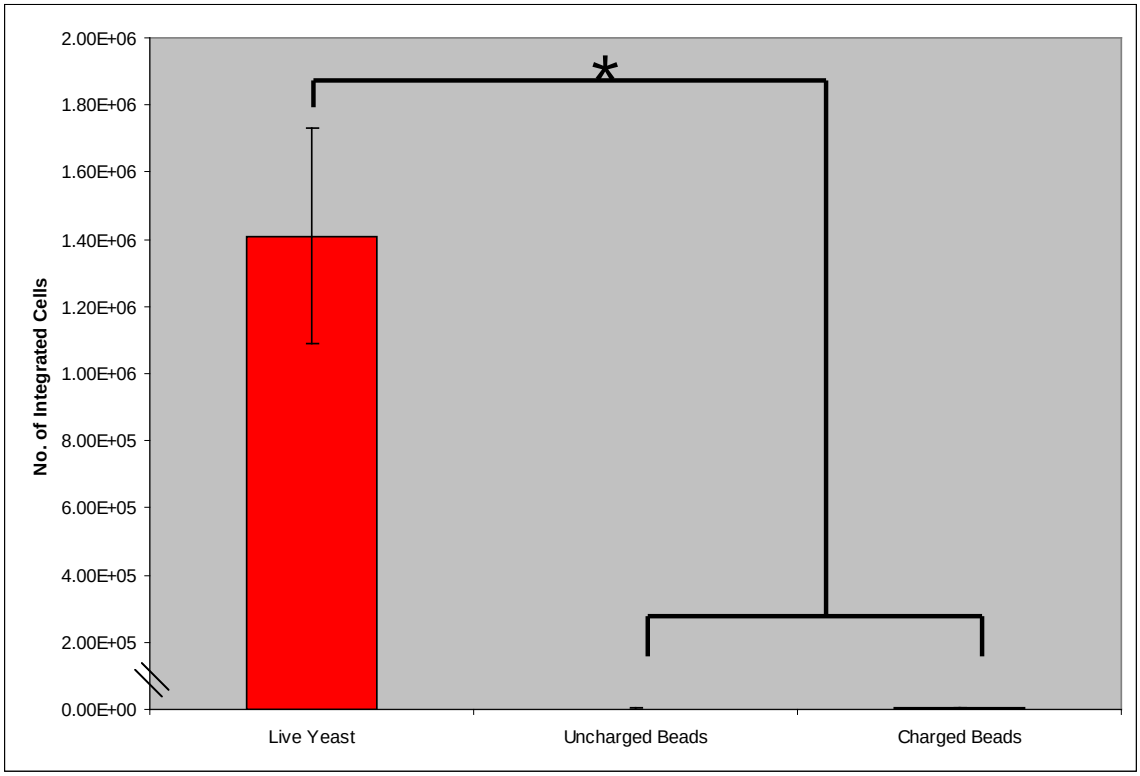

Figure 18. Comparison of integration capability of living cells and cell surrogates. Approximately 10^7 yeast cells stained with SYTO 64 or fluorescent latex beads with the indicated surface charge were added in water to premade *di*C_6PC/silica films and allowed to integrate for 30 minutes at ambient conditions, after which unintegrated cells and beads were removed by rinsing for 10 seconds. The number of integrated cells was then counted using NIS-elements microscopy software. ANOVA with Dunn's Multiple Comparison Post-Test: n=30, *=$p<0.05$. Error bars represent 95% confidence interval.

pH and ionic strength conditions are expected to influence integration through their effects on the silica condensation rate constant as well as their influence on development of osmotic stress. Yeast cells were introduced to a *di*C_6PC/silica film as described above, only being suspended in the indicated buffer solution instead of water. After washing, integrated cells were counted, with the results presented below in Figure 19.

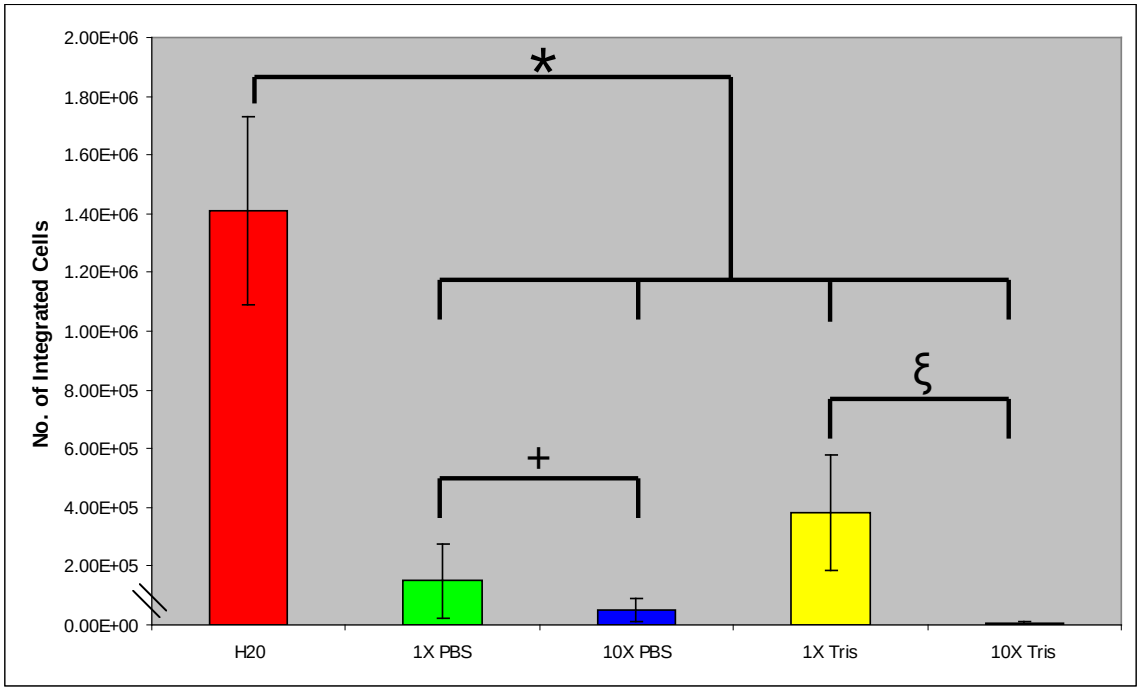

Figure 19. Effects of buffers on cell integration. Approximately 10^7 yeast cells stained with SYTO 64 were added in the indicated buffer to premade *di*C_6PC/silica films and allowed to integrate for 30 minutes at ambient conditions, after which unintegrated cells were removed by rinsing for 10 seconds. The number of integrated cells was then counted using NIS-elements microscopy software. ANOVA with Dunn's Multiple Comparison Post-Test: n = 30, * = $p<0.05$, + = $p<0.05$, ζ = $p<0.05$. Error bars represent 95% confidence interval.

We see a dramatic reduction in the number of cells that are able to integrate when introduced in 1X PBS at pH 7. This number is even further reduced when the buffer capacity is increased to 10X.

It is also known that phosphates can interact with silicates to hinder silica condensation[xviii]. To account for the presence of PBS, a buffer containing no phosphates, Tris, was used. We find that there is a slight increase in the number of cells that are able to integrate in the presence of a buffer that does not contain phosphates. We again obsserve a serious reduction in the number of integrated cells when the buffer strength is increased to 10X. These results are consistent with neutral pH and high ionic strength promoting silica condensation, which, if extensive, should inhibit integration. It could also point out a requirement for a pH gradient for the rearrangement of lipid and silica during integration to occur.

Since the establishment of a pH gradient is suggested to drive the integration of cells into lipid/silica nanostructures, it is clear that active metabolic processes from the cell are also needed. With the necessity of intimate interactions between the cell and the material, the surface of the cell must also play a key role in integration. To confirm these assumptions, various methods were used to alter the cell surface composition as well as the metabolic state of the cell, with the results presented below in Figure 20.

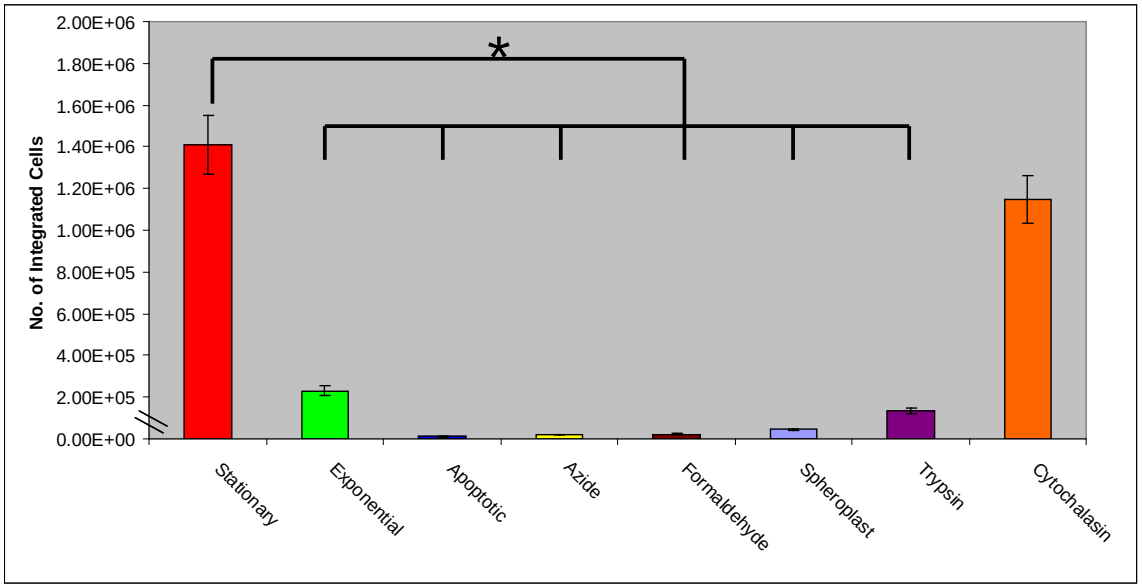

Figure 20. Effects of cell surface composition and metabolic state on cell integration. Approximately 10^7 yeast cells, stained with SYTO 64, in the indicated metabolic state or treated with the indicated chemical using the standard microbiology textbook method were added in the indicated buffer to premade *di*C_6PC/silica films and allowed to integrate for 30 minutes at ambient conditions, after which unintegrated cells were removed by rinsing for 10 seconds. The number of integrated cells was then counted using NIS-elements microscopy software. ANOVA with Dunn's Multiple Comparison Post-Test: n = 30, * = $p<0.05$. Error bars represent 95% confidence interval.

First, yeast were grown out in exponential phase and concentrated to match the stationary-phase standard. After integration and washing, we find that there is a dramatic reduction in the number of exponential-phase cells that are able to integrate compared to stationary phase cells. This is a result of the varying cell metabolism and surface composition found between exponential and stationary growth phases, in which stationary phase cells display a fully-developed cell wall in contrast with the membrane-like cell wall of cells in an exponential growth phase[xix].

To further characterize the effects of the cells' metabolic state on the integration process, cells that have been induced into apoptosis by heat shock were used. It has been shown above that these cells are not able to establish a large external pH gradient and do not effectively interact with the lipid in the host matrix. We find that these cells integrate at numbers at least two orders of magnitude below the standard, which is at the lower detection limit of our microscopic counting technique. This drastic reduction in the ability of cells to integrate shows that in order for cells to integrate they must be in an active metabolic state capable of interaction with the external environment by controlling the pH.

Additionally, we find that chemically altering the metabolic state of the cell can also limit integration ability. ATP production in the cell can be effectively inhibited by the use of sodium azide to decouple the electron transport within the cell's respiratory cycle. When cells were treated with sodium azide prior to integration, we find that very few of the cells are able to integrate, similar to the apoptotic cells. A similar

trend is also observed when cells are fixed with paraformaldehyde. These results confirm the necessity of active metabolic processes to establish a pH gradient and interact with the lipid and silica resulting in integration.

The effects of the cell surface composition can also be investigated by chemically alteration. We have already seen that the change in cell surface between the exponential and stationary growth phases dramatically impacts the integration process. If the cell wall of the stationary phase cell wall is enzymatically removed using zymolase to create spheroplasts, cells are able to integrate in numbers similar to that of the exponential phase cells. This is not surprising, as it has already been shown above that cells are unable to maintain an effective pH gradient with their cell wall removed. This result displays the influence of the stationary phase cell wall and the corresponding ability to control the pH of the surrounding environment during the integration process. This notion is furthered when similar results were obtained for cells that had been treated with trypsin to damage the cell surface proteins. The impaired ability of the cell to interact with the lipid and silica with damaged surface proteins confirms the importance of the interaction of the cell surface with the lipid and silica in order to achieve integration.

A physical attempt by the cell to "burrow" into the film was also investigated. Cytochelasin was used to destroy the actin composing the yeast cytoskeleton. This destroys the cells' ability to perform any directed locomotion. When yeast are treated with cytochelasin before attempting integration, we find that this lack of movement does not impact the integration process. This indicates that the interaction of the cell surface with the lipid and silica is dominant during the integration process.

If the integration process truly requires active processes from the cell, then integration should be influenced by the temperature and resulting metabolic rate of the cells. We find, in Figure 21 below, that the cell metabolic rate does directly influence the number of cells that integrate. At 32ºC, the metabolic rate of the cell is roughly two times the rate at 25ºC. Similarly, we found that the number of cells that integrate approximately doubles at 32ºC. We also find a corresponding decrease in cell integration at lower temperatures. Additionally, we found that the temperature of the film over this same range was not a factor, as we are already well above the transition temperature for this lipid. These results indicate that the interaction of the cell surface with the material and the ability to establish pH gradients to drive integration are clearly manifestations of active cell responses.

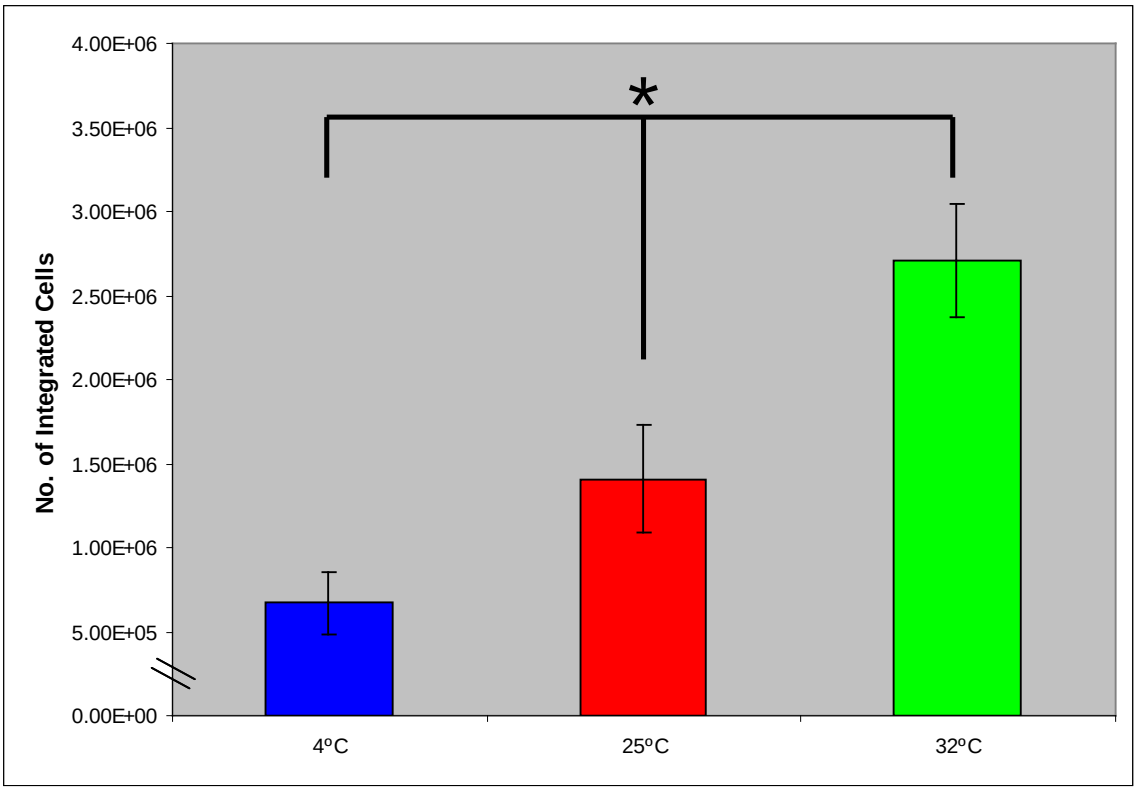

Figure 21. Effects of temperature on cell integration. Approximately 10^7 yeast cells stained with SYTO 64 and maintained at the indicated temperature were added in water to premade *di*C_6PC/silica films and allowed to integrate for 30 minutes at the indicated temperature, after which unintegrated cells were removed by rinsing for 10 seconds. The number of integrated cells was then counted using NIS-elements microscopy software. ANOVA with Dunn's Multiple Comparison Post-Test: n = 30, * = $p<0.05$. Error bars represent 95% confidence interval.

One distinctly interesting observation made during the course of these cell integration experiments is that all cells that were able to integrate appear surprisingly similar. All integrated cells form a distinct pH gradient and a region of localized surfactant, as confirmed by SEM, EDS, and confocal microscopy. This seems to confirm the importance of cellular metabolic behavior and surface interactions with the silica and surfactant in the integration process. Effectively, the only cells that were able to integrate were those that were unaffected by the various treatments.

The previously mentioned data for cell integration was obtained using a system consisting of *di*C_6PC and partially-hydrolyzed TEOS in a high-water sol displaying a relatively slow condensation rate. One main advantage of the cell-directed integration approach is the ability to integrate cells within various nanostructures by varying the type of surfactant template as well as the sol composition. The effects of differing surfactants and sols on the number of cells that are able to integrate are shown below in Figure 22.

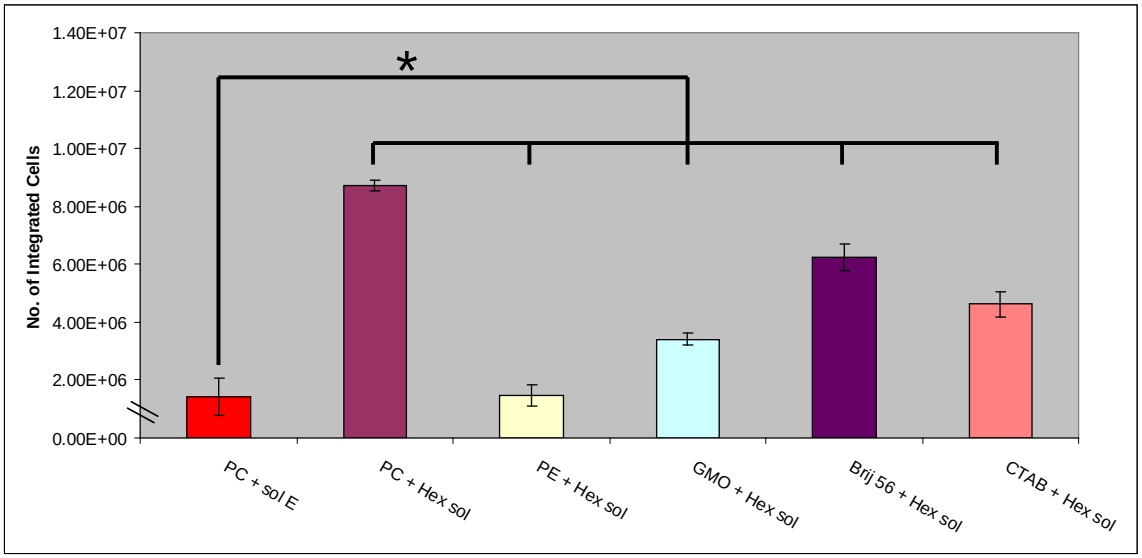

Figure 22. Effects of different lipids and sols on cell integration. Approximately 10^7 yeast cells stained with SYTO 64 were added in water to premade films using different surfactants and silica sol compositions, then allowed to integrate for 30 minutes at ambient conditions, after which unintegrated cells were removed by rinsing for 10 seconds. The number of integrated cells was then counted using NIS-elements microscopy software. ANOVA with Dunn's Multiple Comparison Post-Test: n = 30, * = $p<0.05$. Error bars represent 95% confidence interval.

Besides the aforementioned partially-hydrolyzed TEOS sol (sol E), high-quality ordered nanostructures can also be obtained by using *di*C_6PC with an unhydrolyzed TEOS sol (hex sol). Despite having the same templating molecule and the same nanostructure, these two films do not have similar wetting angles with water. As a result, droplets spread further on the more hydrophilic hex sol system. This effectively increases the surface area of the nanostructure available for interaction with the cells and consequently leads to a higher number of integrated cells.

The hex sol does not contain an abundance of water, and as such can be used to form high quality nanostructures using a variety of surfactant molecules. A variety of molecules were used, including short-chain lipids with different head groups as well as longer chain lipid analogues and traditional surfactants resulting in hexagonal, rhombohedral, and cubic symmetries to integrate cells as mentioned above. We find that the number of cells that are able to integrate into each film is consistent with the wetting angle of the film surface, further demonstrating the importance of intimate contact between the cell, surfactant, and silica in order for the cell to integrate into the material.

If cell integration is dependent on the ability of silica to be differentially hydrolyzed and condensed due to the pH gradient established by the cell, then the extent of condensation of the film prior to the introduction of cells should be a limiting factor. By using various methods to promote silica condensation, it can be shown that cell integration is hindered by increasing the extent of pre-condensed silica in the film.

Concentrated base vapors can be used to enhance the rate of silica condensation without damaging the surfactant molecules. When standard (*di*C_6PC and sol E) films are exposed to 5N NH_4OH vapors for

varying amounts of time, the effects of silica condensation on integration are revealed, as shown below in Figure 23. We find that brief exposures can actually increase the number of cells that are able to integrate. This can be attributed to a decreasing contact angle resulting in more accessible surface area, as mentioned above, and a minimal amount of silica condensation at these short times. At longer times, however, the contact angle stabilizes and the number of integrated cells begins to decrease. This is indicative of the necessity of the cells to interact with uncondensed silica in order to obtain the rearrangement of molecules noted in the integration process.

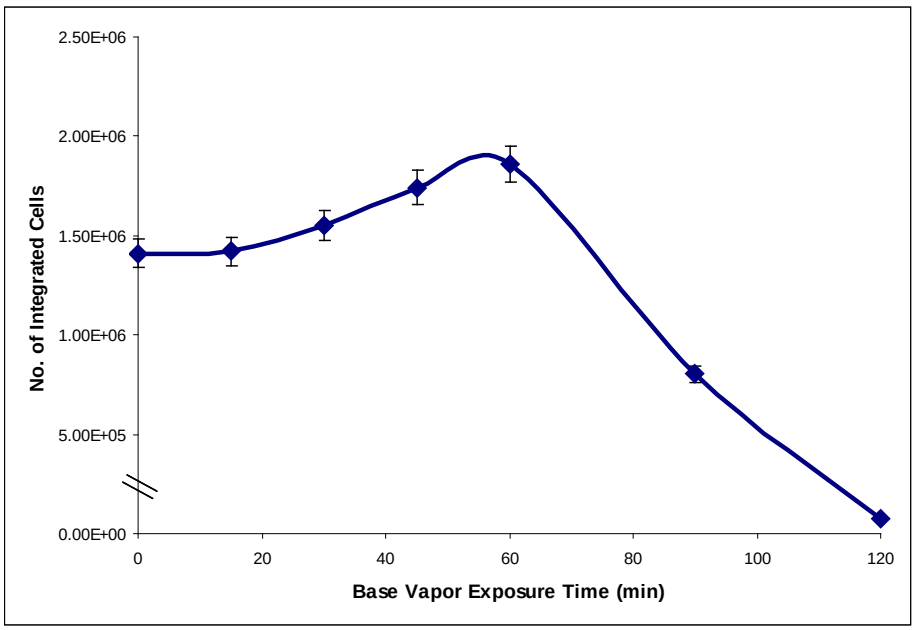

Figure 23. Effects of silica condensation by base vapor exposure on cell integration. Approximately 10^7 yeast cells stained with SYTO 64 were added in water to premade *di*C_6PC/silica films, which had been exposed to saturated ammonium hydroxide vapors for the indicated period of time, and allowed to integrate for 30 minutes at ambient conditions, after which unintegrated cells were removed by rinsing for 10 seconds. The number of integrated cells was then counted using NIS-elements microscopy software. At all time points, n= 12 . Error bars represent 95% confidence interval.

The rate of silica polymerization can be also catalyzed by the presence of UV light. As such, films created using the standard protocol (*di*C_6PC and sol E) were treated in a UV/Ozone reactor (UVO) for varying lengths of time prior to cell integration. The number of cells that were able to integrate into these films is shown below in Figure 24. We find, as for the base vapor exposure, initial exposure results in increased hydrophilicity and leads to higher numbers of integrated cells. Again we see an eventual decrease in the number of integrated cells following the stabilization of wetting angle and further condensation. What is interesting to note, however, is that the surfactant is also being broken down and removed by the ozone during this process. By following this process with IR spectroscopy, we find that the contact angle of the film changes as the surfactant is degraded. The stabilization of the contact angle coincides with the destruction of all template molecules. At this point, however, the silica has not been fully condensed.

After this time, we see a dramatic decrease in the ability of cells to integrate into these films, demonstrating the importance of the interactions between not only the cell and the silica, but also the interactions of the surfactant with the cell and with the silica.

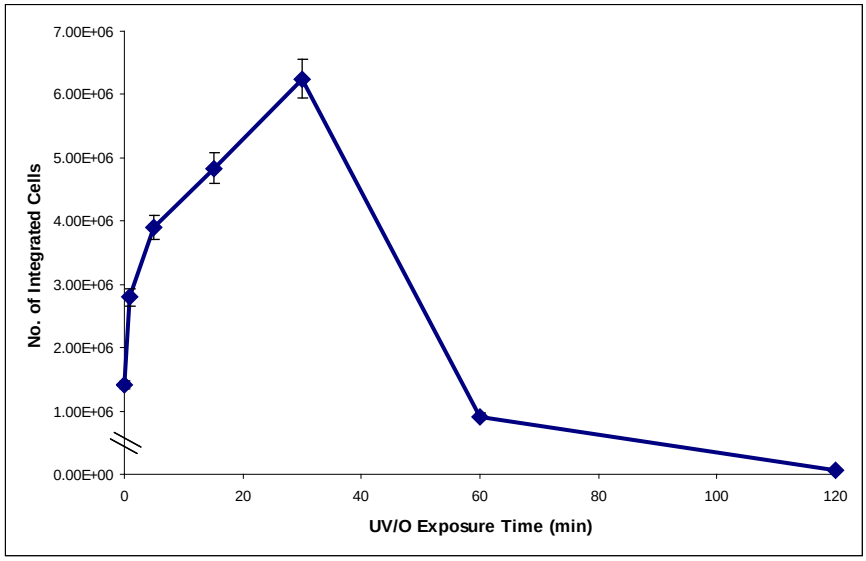

Figure 24. Effects of silica condensation by UV/O exposure on cell integration. Approximately 10^7 yeast cells stained with SYTO 64 were added in water to premade *di*C_6PC/silica films, which had been exposed in a UV/O cleaner to for the indicated period of time, and allowed to integrate for 30 minutes at ambient conditions, after which unintegrated cells were removed by rinsing for 10 seconds. The number of integrated cells was then counted using NIS-elements microscopy software. At all time points, n= 12. Error bars represent 95% confidence interval.

Humidity is an important, yet often overlooked, factor in creating nanostructured silica materials. Silica condensation is promoted by increasing the humidity, allowing more water, a reactant in this case, to access the developing silica network. The effects of humidity and the resulting silica condensation on cell integration were investigated using the standard films (*di*C_6PC and sol E). The number of cells that were able to integrate into films which had been exposed to various humidities over time is shown below in Figure 25.

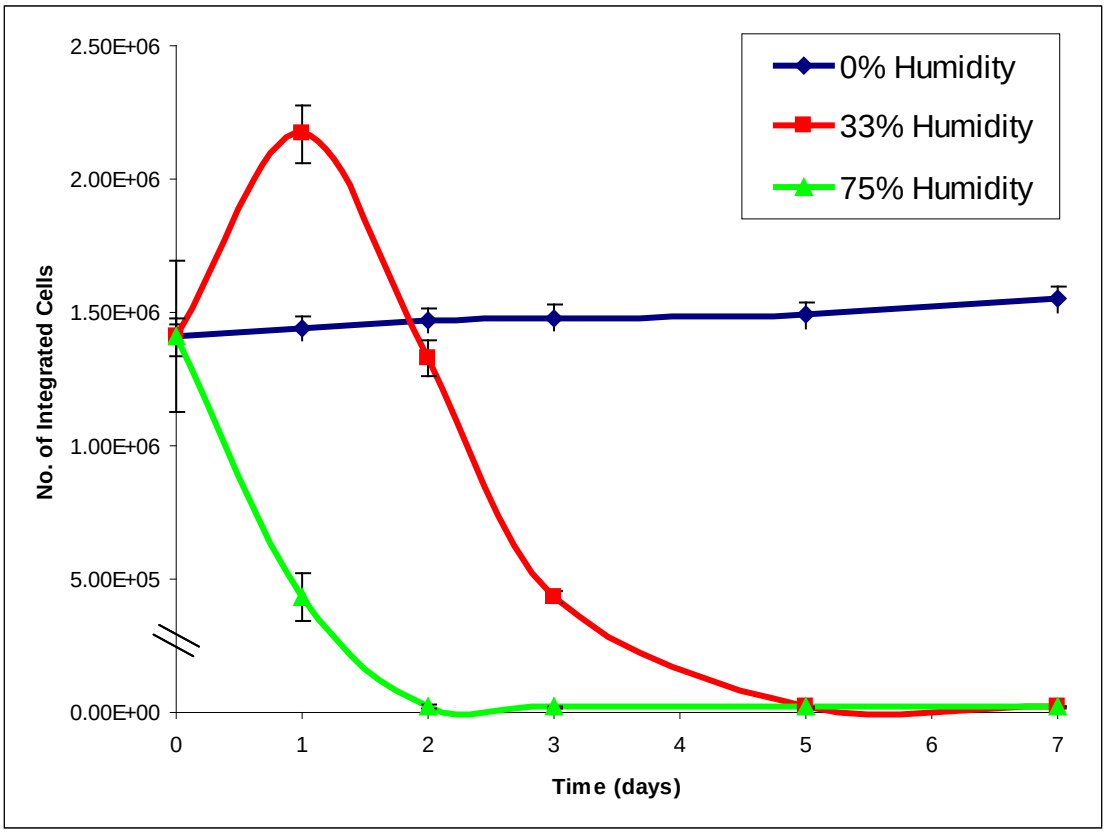

Figure 25. Effects of humidity on cell integration. Approximately 10^7 yeast cells stained with SYTO 64 were added in water to premade *di*C_6PC/silica films, which had been maintained at the indicated humidity for the indicated period of time, and allowed to integrate for 30 minutes at ambient conditions, after which unintegrated cells were removed by rinsing for 10 seconds. The number of integrated cells was then counted using NIS-elements microscopy software. Error bars represent 95% confidence interval.

Again, we find that the amount of cells initially increases due to a decreasing wetting angle. Integration then decreases after stabilization of the contact angle, coinciding with further silica condensation. The time at which the extent of silica condensation begins to hinder the integration process is dependent on the humidity of the environment surrounding the film. By increasing humidity, the rate of silica condensation also increases, resulting in a dramatic decrease in the number of cells that are able to integrate into the films.

Humidity is of great interest when designing a platform for cell-based systems. The effects of humidity on cell integration give us information related to the shelf-life of the nanostructures. For our nanostructured silica films to serve as platforms for these systems, it is obvious and imperative the cells must be able to integrate into the films. This data shows us that these films could be marketed as platforms for cell immobilization and retain an acceptable shelf-life if stored properly in a low-humidity environment that would minimize the hygroscopic nature of the films.

3. Publications and Patents from previous grant cycles (2003-2009):

3.1.1 Refereed Journal Articles, Submitted or Accepted:

3.1.2 Refereed Journal Articles, Published 2003 to 2009:

1 E. C. Carnes, D. M. Lopez, N. P. Donegan, A. Cheung, H. Gresham, G. S. Timmins, and C. J. Brinker, "Confinement-induced quorum sensing of individual Staphylococcus aureus bacteria," Nature Chemical Biology **6** (1), 41-45 (2010).

2 L. N. Zhang, S. Singh, C. S. Tian, Y. R. Shen, Y. Wu, M. A. Shannon, and C. J. Brinker, "Nanoporous silica-water interfaces studied by sum-frequency vibrational spectroscopy," Journal of Chemical Physics **130** (15) (2009).

3 J. W. Liu, A. Stace-Naughton, X. M. Jiang, and C. J. Brinker, "Porous Nanoparticle Supported Lipid Bilayers (Protocells) as Delivery Vehicles," Journal of the American Chemical Society **131** (4), 1354-+ (2009).

4 J. W. Liu, A. Stace-Naughton, and C. J. Brinker, "Silica nanoparticle supported lipid bilayers for gene delivery," Chemical Communications (34), 5100-5102 (2009).

5 J. W. Liu, X. M. Jiang, C. Ashley, and C. J. Brinker, "Electrostatically Mediated Liposome Fusion and Lipid Exchange with a Nanoparticle-Supported Bilayer for Control of Surface Charge, Drug Containment, and Delivery," Journal of the American Chemical Society **131** (22), 7567-+ (2009).

6 D. R. Dunphy, T. M. Alam, M. P. Tate, H. W. Hillhouse, B. Smarsly, A. D. Collord, E. Carnes, H. K. Baca, R. Kohn, M. Sprung, J. Wang, and C. J. Brinker, "Characterization of Lipid-Templated Silica and Hybrid Thin Film Mesophases by Grazing Incidence Small-Angle X-ray Scattering," Langmuir **25** (16), 9500-9509 (2009).

7 E. C. Carnes, J. C. Harper, C. E. Ashley, D. M. Lopez, L. M. Brinker, J. W. Liu, S. Singh, S. M. Brozik, and C. J. Brinker, "Cell-Directed Localization and Orientation of a Functional Foreign Transmembrane Protein within a Silica Nanostructure," Journal of the American Chemical Society **131** (40), 14255-+ (2009).

8 J. B. Pang, S. S. Xiong, F. Jaeckel, Z. C. Sun, D. Dunphy, and C. J. Brinker, "Free-standing, patternable nanoparticle/polymer monolayer arrays formed by evaporation induced self-assembly at a fluid interface," Journal of the American Chemical Society **130** (11), 3284-+ (2008).

9 J. B. Pang, J. N. Stuecker, Y. B. Jiang, A. J. Bhakta, E. D. Branson, P. Li, J. Cesarano, D. Sutton, P. Calvert, and C. J. Brinker, "Directed aerosol writing of ordered silica nanostructures on arbitrary surfaces with self-assembling inks," Small **4** (7), 982-989 (2008).

10 E. Dovgolevsky, S. Kirmayer, E. Lakin, Y. Yang, C. J. Brinker, and G. L. Frey, "Self-assembled conjugated polymer-surfactant-silica mesostructures and their integration into light-emitting diodes," J. Mater. Chem. **18** (4), 423-436 (2008).

11 H. Y. Fan, C. Hartshorn, T. Buchheit, D. Tallant, R. Assink, R. Simpson, D. J. Kisse, D. J. Lacks, S. Torquato, and C. J. Brinker, "Modulus-density scaling behaviour and framework architecture of nanoporous self-assembled silicas," Nat. Mater. **6** (6), 418-423 (2007).

12 G. De, R. Kohn, G. Xomeritakis, and C. J. Brinker, "Nanocrystalline mesoporous palladium

activated tin oxide thin films as room-temperature hydrogen gas sensors," Chemical Communications (18), 1840-1842 (2007).

13 H. K. Baca, E. Carnes, S. Singh, C. Ashley, D. Lopez, and C. J. Brinker, "Cell-directed assembly of bio/nano interfaces - A new scheme for cell immobilization," Accounts of Chemical Research **40**, 836-845 (2007).

14 A. Wright, J. Gabaldon, D. B. Burckel, Y. B. Jiang, Z. R. Tian, J. Liu, C. J. Brinker, and H. Y. Fan, "Hierarchically organized nanoparticle mesostructure arrays formed through hydrothermal self-assembly," Chem. Mat. **18** (13), 3034-3038 (2006).

15 R. Truesdell, A. Mammoli, P. Vorobieff, F. van Swol, and C. J. Brinker, "Drag reduction on a patterned superhydrophobic surface," Phys. Rev. Lett. **97** (4), 4 (2006).

16 S. Singh, J. Houston, F. van Swol, and C. J. Brinker, "Superhydrophobicity - Drying transition of confined water," Nature **442** (7102), 526-526 (2006).

17 A. T. Rodriguez, M. Chen, Z. Chen, C. J. Brinker, and H. Y. Fan, "Nanoporous carbon nanotubes synthesized through confined hydrogen-bonding self-assembly," Journal of the American Chemical Society **128** (29), 9276-9277 (2006).

18 Y. B. Jiang, N. G. Liu, H. Gerung, J. L. Cecchi, and C. J. Brinker, "Nanometer-thick conformal pore sealing of self-assembled mesoporous silica by plasma-assisted atomic layer deposition," Journal of the American Chemical Society **128** (34), 11018-11019 (2006).

19 X. M. Jiang and C. J. Brinker, "Aerosol-assisted self-assembly of single-crystal core/nanoporous shell particles as model controlled release capsules," Journal of the American Chemical Society **128** (14), 4512-4513 (2006).

20 H. Y. Fan, A. Wright, J. Gabaldon, A. Rodriguez, C. J. Brinker, and Y. B. Jiang, "Three-dimensionally ordered gold nanocrystal/silica superlattice thin films synthesized via sol-gel self-assembly," Adv. Funct. Mater. **16** (7), 891-895 (2006).

21 H. Y. Fan, J. Gabaldon, C. J. Brinker, and Y. B. Jiang, "Ordered nanocrystal/silica particles self-assembled from nanocrystal micelles and silicate," Chemical Communications (22), 2323-2325 (2006).

22 C. J. Brinker and D. R. Dunphy, "Morphological control of surfactant-templated metal oxide films," Curr. Opin. Colloid Interface Sci. **11** (2-3), 126-132 (2006).

23 H. K. Baca, C. Ashley, E. Carnes, D. Lopez, J. Flemming, D. Dunphy, S. Singh, Z. Chen, N. G. Liu, H. Y. Fan, G. P. Lopez, S. M. Brozik, M. Werner-Washburne, and C. J. Brinker, "Cell-directed assembly of lipid-silica nanostructures providing extended cell viability," Science **313** (5785), 337-341 (2006).

24 K. Yang, H. Y. Fan, K. J. Malloy, C. J. Brinker, and T. W. Sigmon, "Optical and electrical properties of self-assembled, ordered gold nanocrystal/silica thin films prepared by sol-gel processing," Thin Solid Films **491** (1-2), 38-42 (2005).

25 S. Torquato, A. Donev, A. G. Evans, and C. J. Brinker, "Manufacturable extremal low-dielectric, high-stiffness porous materials," J. Appl. Phys. **97** (12), 5 (2005).

26 S. Gogte, P. Vorobieff, R. Truesdell, A. Mammoli, F. van Swol, P. Shah, and C. J. Brinker, "Effective slip on textured superhydrophobic surfaces," Phys. Fluids **17** (5), 4 (2005).

27 H. Y. Fan, E. W. Leve, C. Scullin, J. Gabaldon, D. Tallant, S. Bunge, T. Boyle, M. C. Wilson, and C. J. Brinker, "Surfactant-assisted synthesis of water-soluble and biocompatible semiconductor

quantum dot micelles," Nano Lett. **5** (4), 645-648 (2005).

28 H. Y. Fan, E. Leve, J. Gabaldon, A. Wright, R. E. Haddad, and C. J. Brinker, "Ordered two- and three-dimensional arrays self-assembled from water-soluble nanocrystal-micelles," Adv. Mater. **17** (21), 2587-+ (2005).

29 H. Y. Fan, Z. Chen, C. J. Brinker, J. Clawson, and T. Alam, "Synthesis of organo-silane functionalized nanocrystal micelles and their self-assembly," Journal of the American Chemical Society **127** (40), 13746-13747 (2005).

30 D. A. Doshi, P. B. Shah, S. Singh, E. D. Branson, A. P. Malanoski, E. B. Watkins, J. Majewski, F. van Swol, and C. J. Brinker, "Investigating the interface of superhydrophobic surfaces in contact with water," Langmuir **21** (17), 7805-7811 (2005).

31 D. A. Doshi, A. M. Dattelbaum, E. B. Watkins, C. J. Brinker, B. I. Swanson, A. P. Shreve, A. N. Parikh, and J. Majewski, "Neutron reflectivity study of lipid membranes assembled on ordered nanocomposite and nanoporous silica thin films," Langmuir **21** (7), 2865-2870 (2005).

32 H. Y. Fan, K. Yang, D. M. Boye, T. Sigmon, K. J. Malloy, H. F. Xu, G. P. Lopez, and C. J. Brinker, "Self-assembly of ordered, robust, three-dimensional gold nanocrystal/silica arrays," Science **304** (5670), 567-571 (2004).

33 K. Yu, B. Smarsly, and C. J. Brinker, "Self-assembly and characterization of mesostructured silica films with a 3D arrangement of isolated spherical mesopores," Adv. Funct. Mater. **13** (1), 47-52 (2003).

34 Y. Yang, Y. F. Lu, M. C. Lu, J. M. Huang, R. Haddad, G. Xomeritakis, N. G. Liu, A. P. Malanoski, D. Sturmayr, H. Y. Fan, D. Y. Sasaki, R. A. Assink, J. A. Shelnutt, F. van Swol, G. P. Lopez, A. R. Burns, and C. J. Brinker, "Functional nanocomposites prepared by self-assembly and polymerization of diacetylene surfactants and silicic acid," Journal of the American Chemical Society **125** (5), 1269-1277 (2003).

35 B. Smarsly, G. Xomeritakis, K. Yu, N. G. Liu, H. Y. Fan, R. A. Assink, C. A. Drewien, W. Ruland, and C. J. Brinker, "Microstructural characterization of polystyrene-block-poly(ethylene oxide)-templated silica films with cubic-ordered spherical mesopores," Langmuir **19** (18), 7295-7301 (2003).

36 N. G. Liu, Z. Chen, D. R. Dunphy, Y. B. Jiang, R. A. Assink, and C. J. Brinker, "Photoresponsive nanocomposite formed by self-assembly of an azobenzene-modified silane," Angew. Chem.-Int. Edit. **42** (15), 1731-1734 (2003).

37 N. G. Liu, R. A. Assink, B. Smarsly, and C. J. Brinker, "Synthesis and characterization of highly ordered functional mesoporous silica thin films with positively chargeable -NH2 groups," Chemical Communications (10), 1146-1147 (2003).

38 N. G. Liu, R. A. Assink, and C. J. Brinker, "Synthesis and characterization of highly ordered mesoporous thin films with -COOH terminated pore surfaces," Chemical Communications (3), 370-371 (2003).

39 A. Gibaud, D. Grosso, B. Smarsly, A. Baptiste, J. F. Bardeau, F. Babonneau, D. A. Doshi, Z. Chen, C. J. Brinker, and C. Sanchez, "Evaporation-controlled self-assembly of silica surfactant mesophases," J. Phys. Chem. B **107** (25), 6114-6118 (2003).

40 G. Garnweitner, B. Smarsly, R. Assink, W. Ruland, E. Bond, and C. J. Brinker, "Self-assembly of an environmentally responsive polymer/silica nanocomposite," Journal of the American Chemical Society **125** (19), 5626-5627 (2003).

41 D. R. Dunphy, S. Singer, A. W. Cook, B. Smarsly, D. A. Doshi, and C. J. Brinker, "Aqueous stability of mesoporous silica films doped or grafted with aluminum oxide," Langmuir **19** (24), 10403-10408 (2003).

42 D. A. Doshi, A. Gibaud, N. G. Liu, D. Sturmayr, A. P. Malanoski, D. R. Dunphy, H. J. Chen, S. Narayanan, A. MacPhee, J. Wang, S. T. Reed, A. J. Hurd, F. van Swol, and C. J. Brinker, "In-situ X-ray scattering study of continuous silica-surfactant self-assembly during steady-state dip coating," J. Phys. Chem. B **107** (31), 7683-7688 (2003).

43 D. A. Doshi, A. Gibaud, V. Goletto, M. C. Lu, H. Gerung, B. Ocko, S. M. Han, and C. J. Brinker, "Peering into the self-assembly of surfactant templated thin-film silica mesophases," Journal of the American Chemical Society **125** (38), 11646-11655 (2003).

3.1.3 Books Edited (2003 to 2009):

1. Annual Review of Nano Research – Volume 2
   Cao, Guozhong and Brinker, C. Jeffrey, editors
   World Scientific Publishing Co. Ltd., Singapore/London, 20081

2. Annual Review of Nano Research – Volume 1
   Cao, Guozhong and Brinker, C. Jeffrey, editors
   World Scientific Publishing Co. Ltd., Singapore/London, 2006

3. Self-Assembled Nanostructured Materials
   Lu, Yunfeng; Brinker, C. Jeffrey; Antonietti, Markus; and Chunli B., editors
   MRS Symposia Proceedings, Volume 775
   Materials Research Society, Pittsburgh, PA, 2003.

3.1.4 Books Chapters Edited (2003 to 2009):

1. Control of Morphology in Mesoporous and Mesostructured Hybrid Materials
   Darren R. Dunphy, Bernd Smarsly, C. Jeffrey Brinker
   in The Supramolecular Chemistry of Organic-Inorganic Hybrid Materials, Knut Rurack, ed, John Wiley & Sons, Inc., Hoboken, NJ. (est May 2009).

2. Photoresponsive Nanocomposite Materials Including Axobenzene-Containing Polysilsesquixane Films and Photoswitched Nanovalves
   Nanguo Liu and C. Jeffrey Brinker
   in Smart Light-Responsive Materials: Azobenzene Containing Polymers and Liquid Crystals, Yue Zhao and Tomiki Ikeda, eds., John Wiley & Sons, Inc., Hoboken, NJ. April 2009.

3. Evaporation-Induced Self-Assembly to functional Nanostructures
   Fan HY; Brinker CJ. in Mesoporous Crystals and Related Nano-Structured Materials. Studies in Surface Science and Catalysis, (Book Series) Vol 148. May 2004.

3.1.5 Proceedings (2003 to 2009):

1. Self-assembled, ordered gold nanocrystal/silica thin films for prism-based surface plasmon resonance sensors. Yang, Kai; O'Brien, Michael J.; Malloy, Kevin J.; Sigmon, Thomas W.; Fan, Hongyou; Lopez, Gabriel P.; Brinker, C. Jeffrey; Sheik-Bahae, Mansoor.

Quantum Electronics and Laser Science Conference (QELS); 2005; v.2, p.1082-1084. Conference: 2005 Quantum Electronics and Laser Science Conference (QELS); May 22-27 2005; Baltimore, MD

2. Surfactant-assisted synthesis of water-soluble and biocompatible semiconductor quantum dot-micelles. Fan, Hongyou; Leve, Erik W.; Scullin, Chessa; Tallant, David; Wilson, Michael C.; Brinker, C. Jeffrey. Progress in Biomedical Optics and Imaging-Proceedings of SPIE; 2005; v.5705, p.92-100. Conference: Nanobiophotonics and Biomedical Applications II; Jan 24-27 2005; San Jose, CA
3. Electrical and optical properties of self-assembled, ordered gold nanocrystal/silica thin films prepared by sol-gel processing. Yang, K; Fan, H; O'Brien, MJ; La Fontaine, S.; Lopez, GP; Malloy, KJ; Brinker, CJ; Sigmon, TW. Proceedings of the Materials Research Society. Micro- and Nanosystems–Materials and Devices 872, 103-108 (2005).
4. Self-assembly and integration of ordered, robust three-dimensional gold nanocrystal/metal oxide superlattices. Fan, H; Yang, K; Gabaldon, JP; Boye, DM; Sigmon, TW; Malloy, KJ; Brinker, CJ; Proceedings of NSTI Nanotech 2005, p. 765-768
5. The Study of interaction of superhydrophobic (SH) materials with fluids using TSM sensors. Kwoun, SJ; Cairncross, R; Lec, RM; Shah, P.; Brinker, C.J. Proceedings of the 2005 IEEE. International, Frequency Control Symposium and Exposition, August 29-31, 2005; p. 78-83

3.1.6 Patents Issued and Applications Filed (2003 to 2009):

Patents issued / allowed:

1 Preparation of Hydrophobic Coatings. U.S. Patent No. 7,485,343 B1, Issued February 3, 2009.

2 Photo-Definable Self-Assembled Materials. U.S. Patent No. 7,332,264 B2, Issued February 19, 2008

3 Fluid Light Guide Having Hydrophobic Aerogel Cladding Layer. U.S. Patent No. 6,983,093, Issued January 3, 2006

4 Prototyping of Patterned Functional Nanostructures. U.S. Patent No. 6,913,832, Issued July 5, 2005

5 Photo-Definable Self-Assembled Materials. U.S. Patent No. 6,808,867 B2, Issued October 26, 2004.

6 Inorganic dual-layer microporous supported membranes. U.S. Patent No. 6,536,604 Issued March 25, 2003

Patent applications filed:

1. **C. Jeffrey Brinker,** Juewen Liu, Xingmao Jiang, Carlee Ashley. Electrostatically Mediated Liposome Fusion and Lipid Exchange with a Nanoparticle-Supported Bilayer for Control of Surface Charge, Drug Containment, and Delivery. UNM-991 Provisional Appl. filed 1/5/2010
2. Juewen Liu, **C. Jeffrey Brinker** and Carlee Ashley. Porous Nanoparticle Supported Lipid Bilayer Nanostructures, UNM-936; Provisional Appl. 61/208,493 filed 2/25/2009
3. **C. Jeffrey Brinker** and Xingmao Jiang. Freezing Assisted Fabrication of Nano Hollow Cubic Metal Spheres. UNM -890; Provisional Appl. 61/207,033 filed 2/5/2009
4. **C. Jeffrey Brinker** and Xingmao Jiang. Azeotropic Distillation Assisted Fabrication of Monsodisperse Hollow Nano Cubes, UNM -891; Provisional Appl. filed 2/8/2010
5. **C. Jeffrey Brinker**, Carlee Ashley, Juewen Liu. Porous Nanoparticle Supported Lipid Bilayer Nanostructure. UNM-936; Provisional Appl. 61/142,495 filed 1/5/2009
6. **C. Jeffrey Brinker** and Xingmao Jiang. An Aerosol Method for Nano Silver-Silica Composite Anti-microbial Agent. UNM-847; Appl. 12/324,318 filed 11/26/2008
7. **C. Jeffrey Brinker,** Ying-Bing Jiang, Joe Cecchi. Ultra-thin microporous/hybrid materials UNM 745 CIP; Appl. 12/271,719, filed 11/14/2008.

8. **C. Jeffrey Brinker and** Kissel, David J.
   A Superhycrophobic Aerogel that does not Require Perfluoro Compounds or Contain any Fluorine. UNM-876; Provisional Appl. 61/077,145 filed 6/30/2008
9. **C. Jeffrey Brinker and** Kissel, David J. Durable polymer/aerogel based superhydrophobic coatings, a composite material. UNM-875; Provisional Appl. 61/077,143 filed 6/30/2008
10. **Carnes, Eric,** Vojo Deretic, DeAnna Lopez, Sharon Master, Graham Timmins, Brinker, C. Jeffrey . Extended Viability Live Vaccine for TB. MC-401; Provisional Appl. 61/132,4000 filed 6/18/2008
11. **Brinker, C. Jeffrey,** Hongyou Fan, Gabriel Lopez. Self-Assembly of Water Soluble Nanocrystals. UNM 653 CIP; Appl. 12/038,037 filed 2/27/2008
12. Jiang, Xingmao and **Brinker, C. Jeffrey.** Highly Active Titanium Oxide Photooxidation catalyst. UNM 0795; 2nd provisional application 61/011,038 filed 1/13/08
13. Doshi, Dhaval; Fan, Hongyou,; Huesing, Nicola; Hurd, Alan; and **Brinker, C.J.** Photo-definable self-assembled materials. UNM 525-Continuation in part, filed December 4, 2007.
14. Jiang, Xingmao., and **Brinker, C. Jeffrey.** An aerogel method for nano silver-silica composite anti-microbial agent. UNM PS-847; provisional application 60/991.380; filed 11/29/07
15. Jiang, YingBing and **Brinker, C. Jeffrey.** Ultra-thin microporous/hybrid membranes made by successive surface activation and reaction. UNM PS-0828; Provisional application 60/988,180, filed 11/15/07
16. Jiang, YB, Cecchi, JL, **Brinker, C.J**. Method of Making Dense, Conformal, Ultra-Thin Cap Layers of Nanoporous Low-k ILD by Plasma-Assisted Atomic Layer Deposition
    UNM-745, provisional application filed 2/13/2006
17. **C. Jeffrey Brinker**; Pratik Shah; Eric D. Branson; Frank van Swol. Processing and Patterning of Hydrophobic Coatings. DOE No./Sandia No. S-103,479/SD-7616, application filed March 2004

3.2 Awards and Honors during previous grant cycles (2003-2009):

3.2.1 PI Awards, C. Jeffrey Brinker

2003 Materials Research Society MRS Medal

2005 University of New Mexico Research Excellence Award

2006 Directeur de Recherche Universite Pierre et Marie Curie, Paris VI

2006 Rutgers University Distinguished Alumnus Award

2007 R&D 100 Award: Self-Assembling Process for Fabricating Tailored Thin Films

2008 R&D100 Award: Patterned Superhydrophobic Surfaces

2008 Edward R. Orton Jr. Memorial Award, American Ceramic Society and ASM

2009 Named Fellow of the Materials Research Society

2010 To receive named Robert B. Sosman Award in Basic Science, American Ceramic Society

3.2.2 Major National and International Graduate Student Awards and Fellowships:

1. Carlee Ashley (PhD 2010) Materials Research Society Fall 2009 Meeting, Graduate Student Silver Award, Boston, MA.
2. Carlee Ashley (PhD 2010), Materials Research Society Fall 2008 Meeting, Top Poster Award, *Targeted in-vitro Drug Delivery to Cancer*, Boston, MA.
3. Jennifer Pelowitz, NSF Interdisiplinary Graduate Research Trainee (IGERT) Fellowship, 2009-2012
4. Patrick Johnson, NSF Interdisiplinary Graduate Research Trainee (IGERT) Fellowship, 2008-2011

5. Carlee Ashley, (PhD 2010) NSF Interdisiplinary Graduate Research Trainee (IGERT) Fellowship, 2007-2009
6. Eric Carnes (PhD 2008), NSF Interdisiplinary Graduate Research Trainee (IGERT) Fellowship, 2006-2008
7. Eric Carnes, Carlee Ashley, NSF Engineering Ethics Pilot Fellowship, 2007-2008
8. Carlee Ashley, Darren Dunphy, Eric Carnes, C. Jeffrey Brinker, Materials Research Society Fall Meeting, Top Poster Award Finalist, 2008, *Self-assembly of Well-Ordered, Close-Packed 2D Arrays of Recombinant Virus-Like Particles that Nucleate the Growth of Inorganic Nanomaterials.*
9. Shisheng Xiong (PhD 2010), Y. Gao, J. Pang, J. Grey, C.Jeffrey Brinker, Materials Research Society Fall Meeting, Top Poster Award Finalist, 2008, *Functional Monolayer Nanoparticle/polymer Composites Formed by EISA at a Fluid Interface*.
10. Carlee Ashley, First Prize, Graduate student Oral Competition, *GISAXS Characterization of 2D Bacteriophage Arrays Deposited via Convective Assembly*, NM Chapter of the American Vacuum Society, May 22, 2007, Albuquerque, NM (paid trip to AVS International Symposium, Seattle, WA, October 2007).
11. Carlee Ashley, Eric Carnes (PhD 2008), Helen Baca, Jeff Brinker. First Prize, Graduate student poster competition *Cell-Directed Assembly of 3-D Bio-Nano Interfaces.* Industrial Advisory Board Meeting of the UNM/RUTGERS/PENN STATE Ceramic and Composite Materials Center (CCMC), March 13, 2007, Albuquerque, NM
12. Yunfeng Lu (PhD 1998), Presidential Early Career Award for Scientists and Engineers (PECASE), 2005.
13. Yunfeng Lu (PhD 1998), American Chemical Society Unilever (Young Investigator) Award in Colloid and Surface Chemistry, 2005
14. Helen K. Baca (PhD 2005), Materials Research Society Student Gold Award, 2005
15. Helen Baca (PhD candidate), National Science and Defense Graduate Fellowship, 2003

3.2.3 Undergraduate Student Awards

1. DeAnna Lopez, First prize, Spectral Image category, Confocal microscope image "Cells Take the Lead", Microscopy Facility Image Competition, Cancer Center Fluorescence Microscopy Facility, University of New Mexico, February 2008, Albuquerque, NM. Published in Life in Print, Science News Online, Jan 26, 2008, vol. 173, no. 4, p. 56.
2. Cynthia Douthit, Second Prize, Undergraduate student poster competition, Examining Integration Techniques using Living Yeast Cells into Self-Assembled Nanostructures, AIChE 2008 Annual Meeting, November 16-21, 2008, Philadelphia, PA.
3. Cynthia M. Douthit, First Prize, Undergraduate student poster competition *Integrating Living Yeast Cells into Patterned Self-Assembled Nanostructures*, Rio Grande Symposium on Advanced Materials -- RGSAM, October 9, 2007, Albuquerque, NM
4. Andrew Collord, Third Prize, Undergraduate student poster competition, *Structure and Aqueous Stability of Surfactant-Templated Porous Films Synthesized using a Hybrid Inorganic/Organic Sol-Gel Precursor*, Rio Grande Symposium on Advanced Materials -- RGSAM, October 9, 2007, Albuquerque, NM
5. DeAnna Lopez, First Prize, Undergraduate Student Poster Competition, *Cell-to-cell communication among nano-confined cells in self-assembled matrices*. Sandia National Laboratories' Student Symposium, Albuquerque, NM , Aug 2, 2007
6. Patrick Johnson, First Prize, Undergraduate Student Poster Competition, *Gecko-Inspired Superadhesives,* Sandia National Laboratories' Student Symposium, Albuquerque, NM , Aug 2, 2007.
7. DeAnna Lopez, First Prize, Undergraduate Student Poster Competition, *Integration of Living Cells within Self-Assembled Nanostructures,* NM Chapter of the American Vacuum Society, May 22, 2007, Albuquerque, NM

4. References

i. Fuqua, W. C., Winans, S. C., Greenberg, E. P. Quorum sensing in bacteria: the LuxR-LuxI family of cell density-responsive transcriptional regulators. *J. Bacteriol.* **176**, 269-275 (1994).

ii. Diggle, S. P., Griffin, A. S., Campbell, G. S., West, S. A. Cooperation and conflict in quorum sensing bacterial populations. *Nature.* **450**, 411-414 (2007).

iii. Redfield, R. J. Is quorum sensing a side effect of diffusion sensing? *Trends Microbiol.* **10**, 365-370 (2002).

iv. Hense, B. A. et al., Does efficiency sensing unify diffusion and quorum sensing *Nat Rev Microbiol.* **5**, 230-239. (2007).

v. Sandoz, K. M., Mitzimberg, S. M., Schuster, M. Social cheating in *Pseudomonas aeruginosa* quorum sensing. *Proc Natl Acad Sci U S A.* **104**, 15876-15881 (2007).

vi. Wang, R., et al., Identification of novel cytolytic peptides as key virulence determinants for community-associated MRSA. *Nature*. **13**, 1510-1514 (2007).

vii. Waters, C.M., Bassler, B.L. QUORUM SENSING: Cell-to-cell communication in bacteria. *Annu Rev Cell Dev Biol.* **21**, 319-346 (2005).

viii. Dunman, P. M., et al. Transcription Profiling-Based Identification of *Staphylococcus aureus* genes regulated by the *agr* and/or *sarA* Loci. *J. Bact.* **183**, 7341-7353 (2001).

ix. Novick, R. P., Autoinduction and signal transduction in the regulation of staphylococcal virulence. *Mol Microbiol.* **48**, 1429-1449 (2003).

x. Baca, H. K., et al. Cell-directed assembly of lipid-silica nanostructures providing extended cell viability. *Science.* **313**, 337-341 (2006).

xi. Lu, Y., et al. Aerosol-assisted self-assembly of mesostructured spherical nanoparticles. *Nature.* **398**, 223-226 (1999).

xii. Baca, H. K., et al., Cell-directed assembly of bio/nano interfaces—a new scheme for cell immobilization. *Acc. Chem. Res.* **40**, 836-845 (2007).

xiii. Shompole, S., et al., Biphasic intracellular expression of *Staphylococcus aureus* virulence factors and evidence for Agr-mediated diffusion sensing. *Mol Microbiol.* **49**, 919-927 (2003).

xiv. Mathesius, U. *et al*. Extensive and specific responses of a eukaryote to bacterial quorum-sensing signals. *Proc. Natl Acad. Sci. USA* **100**, 1444–1449 (2003).

xv. Shiner, E. K., Rumbaugh, K. P. & Williams, S. C. Inter-kingdom signaling: deciphering the language of acyl homoserine lactones. *FEMS Microbiol. Rev.* **29**, 935–947 (2005).

xvi. Jarry, T. M., Memmi, G., Cheung, A. L., The expression of alpha-haemolysin is required for *Staphylococcus aureus* phagosomal escape after internalization in CFT-1 cells. *Cell Micro.* DOI: 10.1111/j.1462-5822.2008.01166.x (2008).

xvii. Rothfork, J. M., et al., Inactivation of a bacterial virulence pheromone by phagocyte-derived oxidants: New role for the NADPH oxidase in host defense. *Proc Natl Acad Sci U S A*. **101**, 13867-13872 (2004).

xviii. Iler, R.K.. The Chemistry of Silica: Solubility, Polymerization, Colloid and Surface Properties and Biochemistry of Silica, 1979. Wiley

xix. Strathern, J. The Molecular Biology of Yeast, 1985, Cold Spring Harbor Laboratories